Manuscript prepared for Earth Syst. Dynam.
with version 5.0 of the LaTeX class copernicus.cls.
Date: 2 November 2014

Contrasting roles of interception and transpiration in the hydrological cycle. Part 1: temporal characteristics over land

L. Wang-Erlandsson[1,2], R. J. van der Ent[1], L. J. Gordon[2], and H. H. G. Savenije[1]

[1]Department of Water Management, Faculty of Civil Engineering and Geosciences, Delft University of Technology, Delft, the Netherlands
[2]Stockholm Resilience Centre, Stockholm University, Stockholm, Sweden

Correspondence to: L. Wang-Erlandsson (l.wang-2@tudelft.nl)

Abstract. Moisture recycling, the contribution of terrestrial evaporation to precipitation, has important implications for both water and land management. Although terrestrial evaporation consists of different fluxes (i.e., transpiration, vegetation interception, floor interception, soil moisture evaporation, and open water evaporation), moisture recycling (terrestrial evaporation-precipitation feedback) studies have up to now only analysed their combined total. This paper constitutes the first of two companion papers that investigate the characteristics and roles of different evaporation fluxes for land-atmosphere interactions. Here, we investigate the temporal characteristics of partitioned evaporation on land, and present STEAM (Simple Terrestrial Evaporation to Atmosphere Model) – a hydrological land surface model developed to provide inputs to moisture tracking. STEAM estimates a mean global terrestrial evaporation of 73 900 $\mathrm{km^3\,year^{-1}}$, of which 59 % is transpiration. Despite a relatively simple model structure, validation shows that STEAM produces realistic evaporative partitioning and hydrological fluxes that compare well with other global estimates over different locations, seasons and land-use types. Using STEAM output, we show that the terrestrial residence time scale of transpiration (days to months) has larger interseasonal variation and is substantially longer than that of interception (hours). Most transpiration occurs several hours or days after a rain event, whereas interception is immediate. In agreement with previous research, our simulations suggest that the vegetation's ability to transpire by retaining and accessing soil moisture at greater depth is critical for sustained evaporation during the dry season. We conclude that the differences in temporal characteristics between evaporation fluxes are substantial and reasonably can cause differences in moisture recycling, which is investigated more in Part 2, the companion paper.

1 Introduction

Terrestrial evaporation is mediated by land-surface properties, rainfall characteristics, and evaporative demand – conditions that humans are modifying at an unprecedented scale (e.g., Crutzen, 2002; Dore, 2005; Gordon et al., 2005; Rockström et al., 2009b; Trenberth, 2011). Understanding evaporation interaction with land and climate is essential, because evaporation holds a key role in regulating hydrological flows as well as atmospheric feedback. One important land-atmosphere mechanism is the contribution of terrestrial evaporation to precipitation through the process of moisture recycling, which has implications for both water and land management. For example, studies have shown that changes in land-use may potentially reduce crop yields through reductions in moisture recycling (Bagley et al., 2012), that irrigation may increase moisture recycling (e.g., Tuinenburg, 2013; Wei et al., 2013), and that livelihoods in some semi-arid regions are particularly vulnerable to changes in upwind moisture source regions (Keys et al., 2012).

Up to now, moisture recycling studies have only analysed total evaporation. However, the partitioning between transpiration, vegetation interception, floor interception, soil moisture evaporation, and open water evaporation depend on land-use and meteorological conditions. For example, interception and soil moisture evaporation are ephemeral (Gerrits et al., 2009), whereas transpiration continues long into the dry season depending on infiltration rates and the capacity of the soil in the root zone to retain moisture. Vegetation that can access deeper soil moisture can therefore maintain evaporation through transpiration beyond what can be sustained by interception alone. Another example is that transpiration ratios (i.e., transpiration as part of total evaporation) can be relatively higher in wet years (compared to dry years), but smaller in wet months (compared to dry months) (Savenije, 2004). The reason is that wet months tend to have high interception preceding transpiration and consuming the already limited energy available for evaporation, whereas wet years tend to receive increased rainfall during the rainy season that stores and transpires into the dry season. Savenije (2004) suggested that these temporal differences of different evaporation fluxes would have different moisture recycling patterns.

Earlier studies of evaporation time scales have analysed the role of soil moisture for drought (e.g., Serafini and Sud, 1987; Delworth and Manabe, 1988), the precipitation persistence in climate modelling (e.g., Koster and Suarez, 1996), as well as the evaporation response time scale to drying soils (e.g., Teuling et al., 2006) and for inter-comparing and improving land surface models (e.g., Lohmann and Wood, 2003; Wang et al., 2006). Scott et al. (1997) described the timescale of evaporation response through convolution representation of precipitation history and applied it on interception, soil evaporation and transpiration globally. Lohmann and Wood (2003) employed a similar approach to compare 16 land surface models and found significant differences in response between models. Nevertheless, the role of evaporation partitioning and evaporation time scales specifically for moisture recycling has not been studied.

Although there have been much efforts in estimating global land evaporation and evaporation partitioning, the actual magnitudes of the different evaporative fluxes remain disputed. Methods to estimate spatially distributed global land evaporation can broadly be grouped into land surface models, remote sensing, reanalysis, and data-upscaling methods. While the latter two generally do not provide evaporation partitioning, the first two methods are highly reliant on the assumed parameters, algorithms, and terminology definitions in order to assess the partitioning. Thus, it is not surprising that the range of reported evaporation partitioning is large. Model-based global mean transpiration ratio estimates range from 38 to 80 % (see Sect. 5 and Table 3).

Validation of spatially and temporally distributed global evaporation partitioning data is challenging, as observational measurements are constrained in space and time, and suffer from uncertainties themselves. Although eddy covariance measurements have often been used in validating modelled total evaporation (e.g., Liu et al., 2012; Miralles et al., 2013; van den Hoof et al., 2013; Bagley et al., 2011) and sporadically used for deriving evaporation (e.g., Jung et al., 2010) and evaporation partitioning (e.g., Czikowsky and Fitzjarrald, 2009), there are still many issues to be resolved: e.g., non-closure of energy balance, location bias, and upscaling (e.g., Twine et al., 2000; Wilson et al., 2002; Chen et al., 2011; Xiao et al., 2012). A combination of isotope measurement techniques and satellite observations were recently used to investigate evaporative partitioning at the river basin and global scale (Jasechko et al., 2013, 2014), leading to high and disputed (Coenders-Gerrits et al., 2014; Schlaepfer et al., 2014; Sutanto et al., 2014) estimates of the transpiration ratio (80–90 %) (see also Sect. 5). In addition, research initiatives such as GEWEX LandFlux-EVAL and ESA WACMOS-ET (e.g., Jiménez et al., 2011; Miralles et al., 2013) that accumulate knowledge through inter-comparing evaporation and evaporation partitioning are still ongoing.

Thus, there remain many difficulties and uncertainties in estimating evaporation partitioning. In particular, the lack of evaporation partitioning data available at the spatial and temporal scale required for moisture tracking might be a reason for the omission of moisture recycling research in the potentially contrasting effects of separated evaporation fluxes.

The research presented here is divided into two separate research papers. The general aim is to investigate the characteristics and roles of different evaporation fluxes to the atmosphere with respect to moisture recycling. This paper (Part 1) analyses the temporal characteristics of partitioned evaporation on land, and presents and evaluates STEAM (Simple Terrestrial Evaporation to Atmosphere Model) — a hydrological land surface model developed and used for the analyses. van der Ent et al. (2014), (hereafter, Part 2), tracks interception and transpiration fluxes in the atmosphere using the WAM-2layers (Water Accounting Model 2-layers) and investigates the resulting moisture recycling patterns.

Specific research questions investigated in this paper relate to the temporal characteristics important for understanding the reasons for evaporation fluxes to produce different moisture recycling patterns: 1) what are the terrestrial residence time scales of evaporation fluxes? 2) how does the timing of precipitation matter for evaporation partitioning? 3) how robust are the temporal characteristics to uncertainties in storage capacities? We use STEAM to model these fluxes. As a relatively simple evaporation model for analysing the relationship between land-use and moisture recycling, STEAM aims to 1) be tailored for coupling with the atmospheric moisture recycling model WAM-2layers, 2) be flexible for land-use change by land-use parametrisation and by including representation of features particularly important for evaporation (e.g., phenology and irrigation), 3) remain simple, transparent, and computationally efficient, and 4) simulate evaporation and evaporation partitioning in line with current knowledge.

2 Model description

STEAM (Simple Terrestrial Evaporation to Atmosphere Model) is a process-based model assuming water balance at grid cell level. Because of our need to properly quantify partitioned evaporation and its seasonal variations, STEAM includes an irrigation module and calculates dynamic seasonal vegetation parameters based on meteorological conditions. For our current research purposes, we have considered it acceptable to disregard groundwater interactions and lateral flows.

STEAM estimates five evaporative fluxes, and is represented by five stocks, see Fig. 1. First, the vegetation interception stock S_v represents canopy and vegetation surface (such as leafs, branches, and stems) that are the first to be wetted by rainfall ($P-P_\mathrm{sf}$). The evaporation from this stock is vegetation interception E_v, and the water exceeding the storage capacity $S_\mathrm{v,\,max}$ is throughfall P_tf. Second, the floor interception stock S_f represents the ground and litter surface which intercepts the throughfall. The evaporation from this stock is floor interception E_f. The remainder is effective precipitation P_eff, which is generated when the storage $S_\mathrm{f,\,max}$ is exceeded. Third, water that subsequently reaches the unsaturated root zone stock S_uz can be evaporated either as soil moisture evaporation E_sm, or be taken up by plant roots and transpire as transpiration E_t. Fourth, the water stock S_w represents open water in the land-use classes water (01:WAT) and wetlands (12:WET), and water below vegetation in the land-use classes wetlands (12:WET) and rice paddies (19:RIC). The water stock is replenished by adding water J_add that prevents dry-out in the absence of lateral flow routines. Water below vegetation also receives P_tf from vegetation. Excess water comprises Q_uz (exceeding $S_\mathrm{uz,\,max}$) from the unsaturated zone and Q_w from the water stock (exceeding $S_\mathrm{w,\,max}$). The last and fifth stock S_snow does not have a limit, and allows snowfall P_sf to accumulate until melting occurs. Snowmelt P_melt is allowed only if there is snow in S_snow. If the daily mean temperature T_mean is above 273 K, P_melt goes directly to the floor interception stock, otherwise it only adds to Q_uz. In case of irrigation, some water is assumed to be spilled to the vegetation I_v, the floor I_f and the water bodies I_w. All notations are listed in Appendix A.

2.1 Potential evaporation

Total evaporation, the sum of vegetation interception E_v, floor interception E_f, transpiration E_t, soil moisture evaporation E_sm, and open water evaporation E_w, is driven by the daily potential evaporation, and restricted by resistances and water availability. The Penman–Monteith equation (Monteith, 1965) is used to estimate the daily potential evaporation $E_\mathrm{p,\,day}$ [$\mathrm{m\,d^{-1}}$], which is formulated as follows:

$$E_\mathrm{p,\,day}(r_\mathrm{a}) = \frac{\delta(R_\mathrm{net}-G)+\rho_\mathrm{a}C_pD_\mathrm{a}/r_\mathrm{a}}{\rho_\mathrm{w}\lambda(\delta+\gamma)} \quad (1)$$

where δ [$\mathrm{kPa\,K^{-1}}$] is the gradient of the saturated vapour pressure function, R_net [$\mathrm{MJ\,m^{-2}\,d^{-1}}$] is the net radiation, G [$\mathrm{MJ\,m^{-2}\,d^{-1}}$] is the ground heat flux, ρ_a [$\mathrm{kg\,m^{-3}}$] is the density of air, C_p [$1.01\times10^{-3}\,\mathrm{MJ\,kg^{-1}\,K^{-1}}$] is the specific heat of moist air at constant pressure, D_a [kPa] is the vapour pressure deficit, ρ_w [$\mathrm{kg\,m^{-3}}$] is the density of water, λ [$\mathrm{MJ\,kg^{-1}}$] is the latent heat of water vaporisation, γ [$\mathrm{kPa\,K^{-1}}$] is the psychrometric constant, and r_a [$\mathrm{d\,m^{-1}}$] is the aerodynamic resistance. Note that r_a is represented by $r_\mathrm{a,\,v}$ for vegetation, $r_\mathrm{a,\,f}$ for floor and $r_\mathrm{a,\,w}$ for water. The calculations of δ, R_net, G, D_a, λ, γ and the different r_a are given in Appendix B1. The potential evaporation $E_\mathrm{p,\,day}$ in Eq. (1) does not include surface stomatal resistance $r_\mathrm{s,\,st}$ for transpiration or surface soil moisture resistance $r_\mathrm{s,\,sm}$ for soil moisture evaporation. Thus, we introduce k (used in Eq. 8, 10, and 11), which is expressed as a function of a surface resistance r_s and an aerodynamic resistance r_a:

$$k(r_\mathrm{s},r_\mathrm{a}) = \left(1+\frac{r_\mathrm{s}}{r_\mathrm{a}}\frac{\gamma}{\delta+\gamma}\right)^{-1}. \quad (2)$$

The surface stomatal resistance $r_\mathrm{s,\,st}$ is calculated based on the Jarvis–Stewart stress function and optimal temperature based on latitude and altitude, see Appendix B2 for details. The soil moisture resistance $r_\mathrm{s,\,sm}$ is applied to soil moisture evaporation and estimated based on the soil moisture content of the top soil layer (Bastiaanssen et al., 2012):

$$r_\mathrm{s,\,sm} = r_\mathrm{s,\,sm,\,min}{\Theta_\mathrm{top}}^{-3} \quad (3)$$

where $r_\mathrm{s,\,sm,\,min}$ is the minimum surface soil moisture resistance assumed as $3.5\times10^{-4}\ \mathrm{d\,m^{-1}}$, and Θ_top [–] is the effective saturation expressed as:

$$\Theta_\mathrm{top} = \frac{\theta_{\mathrm{top},\,n}-\theta_\mathrm{top,\,res}}{\theta_\mathrm{top,\,sat}-\theta_\mathrm{top,\,res}}. \quad (4)$$

Since there is no explicit top soil storage in STEAM, top soil moisture at the present time $\theta_{\mathrm{top},\,n}$ [–] is derived daily, based on the inflow to the unsaturated storage and top soil moisture from the previous day $\theta_{\mathrm{top},\,n-1}$ (Pellarin et al., 2013):

$$\theta_{\mathrm{top},\,n} = \theta_{\mathrm{top},\,n-1}e^{-\Delta n/\chi}+(\theta_\mathrm{sat}-\theta_{\mathrm{top},\,n-1})(1-e^{-P_\mathrm{eff}/y_\mathrm{top}})+\theta_\mathrm{top,\,res} \quad (5)$$

where Δn is the time step of 24 h, $\theta_\mathrm{top,\,res}$ is the volumetric residual soil moisture content assumed as 0.01, y_top is the top soil depth, and χ is the dry out parameter which varies with clay content of the top soil. The assumed y_top is 0.03 m. In Pellarin et al. (2013), the values used for y_top were 0.05 m and 0.1 m, but we considered that a shallower depth is more relevant for estimating soil moisture evaporation stress. The dry out parameter χ is estimated using the following semi-empirical equation:

$$\chi = \frac{y_\mathrm{top}}{0.1}\max\left[\chi_\mathrm{min}, 32\ln(\eta_\mathrm{clay}+174)\right] \quad (6)$$

where η_clay is the clay content [%] and χ_min is the minimum of χ taken as 60 h. This set of equations (Eq. 5 and 6) was tested in semi-arid West Africa, in the type of regions where soil moisture evaporation is most important. Factors not taken into account include solar radiation, the presence of vegetation and the wind velocity (Pellarin et al., 2013).

2.2 Actual evaporation

To simulate actual evaporation at 3 hour time steps (Δt), we first downscale the daily potential evaporation $E_{\mathrm{p,\,day}}$ using the diurnal distribution of ERA-I 3 h evaporation. The downscaled potential evaporation is subsequently used to evaporate moisture in the following logical sequence — vegetation interception, transpiration, floor interception, and soil moisture evaporation:

$$E_{\mathrm{v,\,lu,\,vs}} = E_{\mathrm{v,\,lu,\,vw}} = \min\left(\frac{S_{\mathrm{v,\,lu}}}{\Delta t}, E_{\mathrm{p}}\left(r_{\mathrm{a,\,v}}\right)\right) \tag{7}$$

$$E_{\mathrm{t,\,lu,\,vs}} = \min\left(\frac{S_{\mathrm{uz,\,lu}}}{\Delta t}, \max\left\{0, \left[E_{\mathrm{p}}\left(r_{\mathrm{a,\,v}}\right) - E_{\mathrm{v,\,lu,\,vs}}\right] \cdot k\left(r_{\mathrm{a,\,v}}, r_{\mathrm{s,\,st}}\right)\right\}\right) \tag{8}$$

$$E_{\mathrm{f,\,lu,\,vs}} = \min\left(\frac{S_{\mathrm{f,\,lu}}}{\Delta t}, \max\left[0, E_{\mathrm{p}}\left(r_{\mathrm{a,\,f}}\right) - E_{\mathrm{v,\,lu,\,vs}} - E_{\mathrm{t,\,lu,\,vs}}\right]\right) \tag{9}$$

$$E_{\mathrm{sm,\,lu,\,vs}} = \min\left(\frac{S_{\mathrm{uz,\,lu}}}{\Delta t}, a\right) \tag{10}$$

$$a = \max\left\{0, \left[E_{\mathrm{p}}\left(r_{\mathrm{a,\,f}}\right) - E_{\mathrm{v,\,lu,\,vs}} - E_{\mathrm{t,\,lu,\,vs}} - E_{\mathrm{f,\,lu,\,vs}}\right] \cdot k\left(r_{\mathrm{a,\,f}}, r_{\mathrm{s,\,sm}}\right)\right\}$$

where the first subscript ($_{\mathrm{v}}$, $_{\mathrm{t}}$, $_{\mathrm{f}}$, $_{\mathrm{sm}}$ or $_{\mathrm{w}}$) denotes an individual evaporative flux, the second subscript ($_{\mathrm{lu}}$) the land-use type ID (see Table C1), and the third subscript ($_{\mathrm{vs}}$, $_{\mathrm{vw}}$ or $_{\mathrm{ow}}$) the type of vegetation-water occupancy (see Table C2). Thus, for the fraction of vegetation in water ϕ_{vw} in wetlands and rice paddies, there is no floor interception or soil evaporation. Here, transpiration is preceded by vegetation interception just as for the fraction of vegetation in soil ϕ_{vs}, whereas open water evaporation takes the position of floor interception in the evaporation sequence and is preceded by both vegetation interception and transpiration:

$$E_{\mathrm{t,\,lu,\,vw}} = \min\left(\frac{S_{\mathrm{w,\,lu}}}{\Delta t}, \max\left\{0, \left[E_{\mathrm{p}}\left(r_{\mathrm{a,\,v}}\right) - E_{\mathrm{v,\,lu,\,vw}}\right] \cdot k\left(r_{\mathrm{a,\,v}}, r_{\mathrm{s,\,st}}\right)\right\}\right) \tag{11}$$

$$E_{\mathrm{w,\,lu,\,vw}} = \min\left(\frac{S_{\mathrm{w,\,lu}}}{\Delta t}, \max\left[0, E_{\mathrm{p}}\left(r_{\mathrm{a,\,w}}\right) - E_{\mathrm{v,\,lu,\,vw}} - E_{\mathrm{t,\,lu,\,vw}}\right]\right). \tag{12}$$

For the water land-use type and the fraction of open water ϕ_{ow} in wetlands, evaporation is expressed as:

$$E_{\mathrm{w,\,lu,\,ow}} = \min\left(\frac{S_{\mathrm{w,\,lu}}}{\Delta t}, \max\left[0, E_{\mathrm{p}}\left(r_{\mathrm{a,\,w}}\right)\right]\right). \tag{13}$$

The total of an evaporation flux from wetland (12:WET) or rice paddy (19:RIC) is determined by the weighted sum based on the fractions of vegetation covered soil ϕ_{vs}, vegetation covered water ϕ_{vw}, and open water ϕ_{ow} (see also Table C2):

$$E_{j,\,\mathrm{lu}} = \phi_{\mathrm{lu,\,vs}} E_{j,\,\mathrm{lu,\,vs}} + \phi_{\mathrm{lu,\,vw}} E_{j,\,\mathrm{lu,\,vw}} + \phi_{\mathrm{lu,\,ow}} E_{\mathrm{w,\,lu,\,ow}} \tag{14}$$

where $E_{j,\,\mathrm{lu}}$ is an evaporation flux ($_j$ denotes $_{\mathrm{v}}$, $_{\mathrm{t}}$, $_{\mathrm{f}}$, $_{\mathrm{sm}}$, or $_{\mathrm{w}}$) of the land-use type $_{\mathrm{lu}}$.

Subsequently, the total of an evaporation flux from a grid cell is determined by the weighted sum of the land-use types:

$$E_j = \sum_{\mathrm{lu}=1}^{\mathrm{lu}=19} \phi_{\mathrm{lu}} E_{j,\,\mathrm{lu}} \tag{15}$$

where ϕ_{lu} is the land-use occupancy fraction of the land-use type $_{\mathrm{lu}}$.

2.3 Phenology

The growing season index i_{GS} (Jolly et al., 2005) varies between 0 and 1, and is used to determine the seasonal variations of leaf area i_{LA}. We formulate i_{GS} in STEAM as follows:

$$i_{\mathrm{GS}} = f\left(T_{\mathrm{min}}\right) f\left(N\right) f\left(\theta_{\mathrm{uz}}\right), \tag{16}$$

where $f(T_{\mathrm{min}})$ is the stress function of minimum temperature, $f(N)$ is the stress function of day length, and $f(\theta_{\mathrm{uz}})$ is the stress function of soil moisture. Note that $f(\theta_{\mathrm{uz}})$ is a modification of the original expression for i_{GS}, where vapour pressure deficit D_{a} was used as a proxy for soil moisture (Jolly et al., 2005). However, since soil moisture is calculated in STEAM, it makes sense to use the soil moisture stress function to replace the original vapour pressure stress function. The stress functions are expressed as:

$$f\left(T_{\mathrm{min}}\right) = \begin{cases} 0 & T_{\mathrm{min}} \leq T_{\mathrm{min,\,low}} \\ \frac{T_{\mathrm{min}} - T_{\mathrm{min,\,low}}}{T_{\mathrm{min,high}} - T_{\mathrm{min,low}}} & T_{\mathrm{min,high}} > T_{\mathrm{min}} > T_{\mathrm{min,low}}, \\ 1 & T_{\mathrm{min}} \geq T_{\mathrm{min,high}} \end{cases} \tag{17}$$

$$f\left(N\right) = \begin{cases} 0 & N \leq N_{\mathrm{low}} \\ \frac{N - N_{\mathrm{low}}}{N_{\mathrm{high}} - N_{\mathrm{low}}} & N_{\mathrm{high}} > N > N_{\mathrm{low}}, \\ 1 & N \geq N_{\mathrm{high}} \end{cases} \tag{18}$$

$$f\left(\theta_{\mathrm{uz}}\right) = \begin{cases} 0 & \theta_{\mathrm{uz}} \leq \theta_{\mathrm{uz,\,wp}} \\ \frac{(\theta_{\mathrm{uz}} - \theta_{uz,\,\mathrm{wp}})(\theta_{\mathrm{uz,\,fc}} - \theta_{\mathrm{uz,\,wp}} + c_{\mathrm{uz}})}{(\theta_{\mathrm{uz,\,fc}} - \theta_{\mathrm{uz,\,wp}})(\theta_{\mathrm{uz}} - \theta_{\mathrm{uz,\,wp}} + c_{\mathrm{uz}})} & \theta_{\mathrm{uz,\,wp}} < \theta_{\mathrm{uz}} < \theta_{\mathrm{uz,\,fc}}, \\ 1 & \theta_{\mathrm{uz}} \geq \theta_{\mathrm{uz,\,fc}} \end{cases} \tag{19}$$

where the lower sub-optimal minimum temperature $T_{\mathrm{min,\,low}}$ is 271.15 K, and the higher $T_{\mathrm{min,\,high}}$ is 278.15 K. The lower sub-optimal threshold day length N_{low} is assumed to be 36 000 s, and the higher N_{high} is 39 600 s (Jolly et al., 2005). T_{min} is taken from the coldest 3 h ERA-I temperature of the day. Calculation of day length N follows the approach of Glarner (2006). The soil moisture stress parameter c_{uz} is fixed at 0.07 (Matsumoto et al., 2008). The soil moisture content θ_{uz} is $S_{\mathrm{uz}}/y_{\mathrm{uz}}$, where y_{uz} [m] is the depth of the unsaturated root zone. The soil moisture contents at wilting point $\theta_{\mathrm{uz,wp}}$ and at field capacity $\theta_{\mathrm{uz,fc}}$ depend on soil type. To prevent unrealistically unstable fluctuations in leaf area, the mean $i_{\mathrm{GS,21}}$ of the past 21 days is used to scale i_{LA} between the land-use type dependent $i_{\mathrm{LA,max}}$ and $i_{\mathrm{LA,min}}$ (Jolly et al., 2005):

$$i_{\mathrm{LA}} = i_{\mathrm{LA,min}} + i_{\mathrm{GS,21}} \left(i_{\mathrm{LA,max}} - i_{\mathrm{LA,min}} \right). \tag{20}$$

2.4 Storage capacities

The storage capacity determines the maximum water availability for the evaporation flux of concern. We derived vegetation interception storage capacity $S_{\mathrm{v,\,max}}$ [m] from the monthly i_{LA} based on the storage capacity factor c_{sc} of roughly 0.2 reported by, for example, de Jong and Jetten (2007) and used in van den Hoof et al. (2013):

$$S_{\mathrm{v,\,max}} = c_{\mathrm{sc}} c_{\mathrm{AR}} i_{\mathrm{LA}}, \tag{21}$$

where c_{AR} is the area reduction factor introduced to compensate for rainfall heterogeneity in space and time. The relationship between i_{LA} and vegetation interception storage varies with vegetation type and a strong relationship has not yet been established. In fact, Breuer et al. (2003) even suggests that no general relationship can be established across vegetation types due to the inherent differences in vegetation structures. Nevertheless, vegetation stock linked to i_{LA} has proven to be useful in many cases where there is a lack of detailed vegetation information.

We assume c_{AR} to be 0.4 for STEAM running with a 3 h time step at the $1.5°$ scale. Area reduction factors have been developed to establish a relationship between average precipitation and extreme precipitation of a region, but can be analogously used to reduce interception storage capacity. In an example diagram obtained from catchment analyses (Shuttleworth, 2012), areas larger than $10\,000\,\mathrm{km}^2$ have an area reduction factor up to approximately 0.6. In STEAM, grid cell areas with $1.5°$ resolution are $10\,000\,\mathrm{km}^2$ already at $68°$ N, and grow to almost $28\,000\,\mathrm{km}^2$ at the equator. Ideally, c_{AR} should vary with the area considered and rainfall duration, but due to a lack of well-established functions, we consider $c_{\mathrm{AR}} = 0.4$ to be acceptable.

The floor interception storage capacity $S_{\mathrm{f,\,max}}$ [m] is modelled as a function of the leaf area and a certain base value:

$$S_{\mathrm{f,\,max}} = c_{\mathrm{sc}} c_{\mathrm{AR}} \left[1 + 0.5 \left(i_{\mathrm{LA,max}} + i_{\mathrm{LA,min}} \right) \right]. \tag{22}$$

The floor storage capacity increases in areas with vegetation, due to litter formation from fallen leafs. A base value is considered, because wetting of the surface always occurs irrespective of the land cover. However, litter is assumed to have been removed in croplands (i.e., 13:CRP, 15:MOS, 18:IRR, and 19:RIC). Thus, $S_{\mathrm{f,\,max}}$ [m] for crops corresponds to that of the litter-free floor:

$$S_{\mathrm{f,\,max,\,crops}} = c_{\mathrm{sc}} c_{\mathrm{AR}}. \tag{23}$$

As a result of the large grid scale (reflected in the area reduction factor), interception storage in STEAM is smaller than normally found in point scale field studies. For example, the vegetation interception storage capacity at the maximum i_{LA} of 5.5 is $0.44\,\mathrm{mm}$, which is about a third of the $1.2\,\mathrm{mm}$ reported in a summer temperate forest (Gerrits et al., 2010) and a fraction of the 2.2 to $8.3\,\mathrm{mm}$ per unit of crown projected area in a tropical rainforest site (Herwitz, 1985).

The storage capacity of the unsaturated root zone $S_{\mathrm{uz,\,max}}$ is assumed to reach field capacity when:

$$S_{\mathrm{uz,\,max}} = \theta_{\mathrm{fc}} y_{\mathrm{uz}}. \tag{24}$$

The $S_{\mathrm{uz,max}}$ is modelled as a function of soil texture and land-use based rooting depth. This is a simplification as many other factors govern root water uptake, including topography (Gao et al., 2013), soil properties, hydraulic redistribution of soil water by roots (Lee et al., 2005), groundwater table (Miguez-Macho and Fan, 2012), and climate (Feddes et al., 2001). In addition, variations of rooting distribution (e.g., Jackson et al., 1996) and the existence of deep roots (e.g., Canadell et al., 1996; Kleidon and Heimann, 2000) may conflict with the assumption of one rooting depth parameter per land-use type.

2.5 Irrigation

STEAM includes irrigation because it has been shown to constitute an important moisture source to the atmosphere (e.g., Gordon et al., 2005; Lo and Famiglietti, 2013; Tuinenburg, 2013; Wei et al., 2013). Irrigation water supplied is assumed to meet the irrigation requirement and is not restricted by water availability. Net irrigation enters the unsaturated zone and is estimated as a function of soil moisture. In rice paddies (19:RIC), irrigation water simply upholds a $10\,\mathrm{cm}$ water level. For non-rice crops (18:IRR), irrigation requirement I_{req} is the amount of water needed to reach field capacity in the unsaturated root zone:

$$I_{\mathrm{req}} = \max\left[0, \frac{y_{\mathrm{uz}}\left(\theta_{\mathrm{uz,\,fc}} - \theta_{\mathrm{uz}}\right)}{\Delta t} - \frac{S_{\mathrm{uz,\,lu}}}{\Delta t}\right]. \tag{25}$$

However, because a certain amount of irrigation water applied is always lost due to inefficiencies in the system, an irrigation efficiency should be applied in order to correctly estimate runoff and water withdrawal. In STEAM, we assume the gross irrigation I_{g} to be twice the I_{req}. Although irrigation efficiency in practice varies greatly with irrigation technique, crop type and country (Rohwer et al., 2007), we consider our simplification acceptable since the gross irrigation assumption affects evaporation (our major concern) less than, e.g., runoff and water withdrawal. Of gross irrigation applied to irrigated non-rice crops (18:IRR), 15 % is directed to the vegetation interception stock S_{v}, and 85 % to the floor interception stock S_{f}. Of the gross irrigation applied to rice paddies (19:RIC), 5 % is directed to vegetation interception stock S_{v}, 5 % to the floor interception stock S_{f} (assuming inter-paddy pathways), and 90 % to the water stock S_{w}.

3 Data

Meteorological data were taken from the ERA-Interim reanalysis (ERA-I) produced by the European Centre for Medium-Range Weather Forecasts (ECMWF) (Dee et al., 2011). We used evaporation, precipitation, snowfall, snowmelt, temperature at 2 m height, dew point temperature at 2 m height, wind speed in two directions at 10 m height, incoming shortwave radiation, and net longwave radiation. All meteorological forcings are given at 3 h and 1.5° latitude × 1.5° longitude resolution. The data used covers latitudes from 57° S to 79.5° N for the years 1985–2009.

The monthly varying land-surface map used in STEAM consists of 19 land-use types, see Table C1. The first 17 International Geosphere Biosphere Programme (IGBP) land-use types are based on the Land Cover Type Climate Modeling Grid (CMG) MCD12C1 created from Terra and Aqua Moderate Resolution Imaging Spectroradiometer (MODIS) data (Friedl et al., 2010) for the year 2001. The two irrigated land-use classes are based on the dataset of Monthly Irrigated and Rainfed Crop Areas around the year 2000 (MIRCA2000) V1.1. (Portmann et al., 2010). The resolution for MODIS is 0.05° and for MIRCA2000 5′. To create the joint map, monthly irrigated land from MIRCA2000 were taken to replace primarily MODIS cropland fraction (13:CRP), and secondarily MODIS cropland/natural mosaic fraction (15:MOS). The joint map has a total land area of 133 146 465 km^2 and includes inland waters except big lakes.

Soil texture data has been taken from the Harmonized World Soil Database (HWSD) (FAO/IIASA/ISRIC/ISSCAS/JRC, 2012) and we assigned volumetric soil moisture content at saturation, field capacity and wilting point based on the United States Department of Agriculture (USDA) soil classification (Saxton and Rawls, 2006). Top soil saturation, subsoil field capacity and subsoil wilting point have been assigned to the original 30″ resolution, and scaled up to 1.5° by area weighing.

For evaporation evaluation, we used the LandFlux-EVAL evaporation benchmark products (Mueller et al., 2013) for the years 1989–2005. This data product consists of a merged synthesis from 5 satellite or observation-based datasets, 5 land-surface model simulations, and 4 reanalysis datasets. For runoff evaluation, composite and model runoff fields from the Global Runoff Data Centre (GRDC) were used (Fekete et al., 2000). The model runoff fields are the simulations of the GRDC Water Balance Model (GRDC-WBM), whereas the composite runoff fields (GRDC-Comp) are the model runoff corrected by observed inter-station discharge (Fekete et al., 2000). In addition, we also used ERA-I runoff fields (Balsamo et al., 2011) in our comparison. It should be noted that the ERA-I runoff fields form a separate dataset that does not directly correspond to ERA-I precipitation minus evaporation. The river basin map is based on the global 30-min drainage direction map of Döll and Lehner (2002).

4 Methods

4.1 Model evaluation

The model evaluation comprises the following model output: total and land-use based evaporation, total and land-use based evaporation partitioning, runoff, irrigation, and irrigation evaporation contribution. Total global fluxes are calculated based on a land area of 133 146 465 km^2 (including Greenland and excluding Antarctica) and for the years 1999–2008. Land-use evaporation is obtained from Eq. 14. Irrigation evaporation contribution was calculated based on the difference in evaporation between STEAM simulations with and without the irrigation routine turned on. Runoff Q from STEAM has been derived from subtracting mean evaporation and mean snow storage changes from mean precipitation:

$$\overline{Q} = \overline{P} - \overline{E} - (\overline{\mathrm{d}S_{\mathrm{snow}}}/\mathrm{d}t). \tag{26}$$

Snow storage changes were subtracted because snow accumulated in glaciers may carry over storage from year to year. Otherwise, most storage changes may be neglected at an annual time scale. Then runoff comparison includes two additional STEAM scenarios: one simulation without irrigation (because irrigation is not always included in land surface models), and one with 5 % uniform reduction in precipitation forcing (because ERA-I precipitation forcing is higher than several other precipitation datasets, see Appendix D).

4.2 Characterisation of partitioned evaporation fluxes

4.2.1 Time scales of evaporation fluxes

The time scales τ_{ts} of the evaporation fluxes is defined as the mean stock over the mean flux rate of concern j:

$$\tau_{\mathrm{ts},\,j} = \frac{\overline{S_j}}{\overline{E_j}}. \tag{27}$$

Figure 1 shows the stock of origin for each evaporation flux. Because both E_{sm} and E_{t} come from S_{uz}, we assumed a stock of soil moisture evaporation $S_{\mathrm{uz,\,sm}}$ and a stock of transpiration $S_{\mathrm{uz,\,t}}$. To obtain $S_{\mathrm{uz,\,sm}}$, we multiplied θ_{top} with the assumed top soil depth y_{top}. To obtain the stock $S_{\mathrm{uz,\,t}}$, $S_{\mathrm{uz,\,sm}}$ was subtracted from the total water available in the unsaturated zone S_{uz}:

$$S_{\mathrm{uz,\,t}} = S_{\mathrm{uz}} - S_{\mathrm{uz,\,sm}} = \theta_{\mathrm{uz}} y_{\mathrm{uz}} - \theta_{\mathrm{top}} y_{\mathrm{top}}. \tag{28}$$

Because the time scale becomes infinite when the flux approaches zero, time scales are not given for areas where the mean evaporation flux is below 0.01 $\mathrm{mm\,d^{-1}}$. Coastal areas where the land area fraction is less than 100 % were removed from the time scale analysis. The time scale for open water evaporation was not calculated.

4.2.2 Evaporation partitioning: time since precipitation

We are interested in how evaporation partitioning evolves with time after precipitation ceases. To do this, we grouped each grid cell at every time step in categories depending on the time that has past since precipitation. Grid cells at a certain time step that has not received precipitation since n time steps back are placed in the (n+1)$^{\text{th}}$ category. Subsequently, evaporation partitioning for each category was retrieved from the model simulation.

In addition, the importance of the evaporation partitioning in relation to rainfall also depends on the evaporated quantity. Thus, we present the portion of evaporation flux during rainy or dry conditions by using evaporation efficiencies β_{wet} and β_{dry} as measures:

$$\beta_{\mathrm{wet,j}} = \frac{\sum E_{wet,j}}{\sum E_j}, \qquad \beta_{\mathrm{dry,j}} = \frac{\sum E_{dry,j}}{\sum E_j}. \tag{29}$$

Here, β_{wet} represents the mean annual portion of an evaporation flux that evaporates during a 3 hour time step with precipitation, and β_{dry} represents the mean annual portion of an evaporation flux that evaporates after experiencing more than 24 hours of no precipitation. To qualify as a wet time step, a 3 hour time step must have $>$0.01 mm precipitation. The subscript $_{\mathrm{j}}$ denotes the evaporation flux of concern. Construction of these evaporation efficiency measures is useful for answering questions such as: how much of total vegetation interception occurs during rainy periods?

4.2.3 Robustness

Large uncertainties exist in evaporation partitioning and estimation of storage capacities. To verify how robust or sensitive the temporal characteristics are to these uncertainties, we performed a sensitivity analysis with two scenarios: transpiration-plus and interception-plus. In transpiration-plus, the unsaturated zone storage capacity increased by 20 % and the vegetation and floor interception storage capacity decreased by 50 %. In interception-plus, the increase and decrease in the storages are reversed, see Table 5.

5 Results: model evaluation

5.1 Total evaporation

STEAM estimates global annual terrestrial evaporation as 555 $\mathrm{mm\,year^{-1}}$ (i.e., 73 900 $\mathrm{km^3\,year^{-1}}$), spatial distribution is shown in Fig.2. This is comparable to current global evaporation datasets. In the Water Model Intercomparison Project (WaterMIP), the range of evaporation given by eleven models was 415–585 $\mathrm{mm\,year^{-1}}$ for the period 1985–1999 forced with WATCH meteorological data (Haddeland et al., 2011). By subtracting global runoff from precipitation products for the years 1984–2007, Vinukollu et al. (2011) arrived at global evaporation rates of 488–558 $\mathrm{mm\,year^{-1}}$ (i.e., 64 000–73 000 $\mathrm{km^3\,year^{-1}}$). In the LandFlux-EVAL multi-data set synthesis, the global mean evaporation was 493 $\mathrm{mm\,year^{-1}}$ as given by a combination of land-surface model simulations, observational dataset, and reanalysis data for both the period of 1989–1995 and 1989–2005 (Mueller et al., 2013).

Figure 3 shows how STEAM evaporation compares to the LandFlux-EVAL product for 1989-2005. STEAM evaporation is within the inter-quartile range of all LandFlux-EVAL products in the tropics, the United States, parts of Europe, South Asia, northern Russia and large parts of Africa south of Sahel. The upper quartile is mostly exceeded in the boreal forests in the northern latitudes, China, Argentina and the Sahel. Most exceedance of STEAM evaporation is in comparison with the land surface models, and the least with the reanalyses data included in the LandFlux-EVAL product. Only a few limited patches in northern Canada, Sudan, Argentina and northern China exceed the LandFlux-EVAL maximum. Seasonally, Fig. 4 shows that Northern Hemisphere spring and summer are generally more in range compared to winter and fall, when STEAM tends to have higher evaporation rates in the northernmost latitudes compared to LandFlux-EVAL. However, LandFlux-EVAL excluded some high evaporation values in the northern latitudes based on physical constraints (Mueller et al., 2013), which consequently eliminates potentially important winter time interception (Schlaepfer et al., 2014).

Evaporation contributions per land-use type are listed in Table 1, and compared to the other studies in Table 2. The highest evaporation rates are found in irrigated lands, evergreen broadleaf forests, and open waters. This is followed by wetlands, savannahs, deciduous broadleaf forests, natural mosaics, woody savannahs, mixed forests, and rainfed croplands. Evaporation rates in the lower tier include contributions from needleleaf forests, grasslands, and shrublands. In general, STEAM evaporation is comparable to the estimates of Gordon et al. (2005), the compilation results of Schlesinger and Jasechko (2014) (based on Mu et al., 2011), and the field data from Rockström et al. (1999). The mixed forest evaporation estimate in STEAM is double that of Gordon et al. (2005), but the area is also very different, suggesting substantial differences in forest definition. Closed shrublands in STEAM also produces higher evaporation rates, but because the numbers are for shrublands in general and not closed shrublands in particular, the shrublands comparison is inevitably inconclusive. Some caution is warranted in comparing evaporation rates across studies. Nevertheless, this comparison shows that evaporation estimates in STEAM are within the range of previous estimates.

5.2 Evaporation partitioning

In STEAM, the dominating evaporation flux is transpiration E_{t} (59 %), followed by vegetation interception E_{v} (21 %), floor interception E_{f} (10 %), soil moisture evaporation E_{sm}

(6 %) and lastly, open water evaporation E_w (4 %). The global distribution of the annual mean evaporation fluxes is shown in Figs. 2 and 5 (as percentage of total evaporation). Seasonal variations of evaporation fluxes are shown over latitudes in Fig. 6. It is shown that transpiration dominates in the densely vegetated areas in the tropics. In addition, transpiration rates increase over the boreal forests during the Northern Hemisphere summer.

Table 3 provides an overview of evaporative partitioning values in the literature and in STEAM. We note that the STEAM global mean transpiration ratio is in good agreement with the literature compilation results presented by Schlesinger and Jasechko (2014) and the LPJ estimate by Gerten et al. (2005), but higher than other land-surface model simulations (Alton et al., 2009; Lawrence et al., 2007; Choudhury et al., 1998; Dirmeyer et al., 2006). Jasechko et al. (2013, 2014) estimated the transpiration ratio to be 80–90 % using a combination of isotope measurement techniques and satellite observations at river basin and the global scales. However, their results have been challenged by Coenders-Gerrits et al. (2014) who showed that the transpiration ratio reduces to 35–80 % by using other input data, Schlesinger and Jasechko (2014) who estimated the global transpiration ratio to be 61 % based on literature data compilation, and by Schlaepfer et al. (2014) who argued that Jasechko et al. (2013)'s underlying assumption that isotope ratios of a lake would be representative for the entire catchment is flawed. A number of possible explanations for the high transpiration ratio bias in isotope studies is also offered by Sutanto et al. (2014).

Table 1 shows the annual average evaporation fluxes as a percentage of total evaporation per land-use class. Transpiration is the dominant evaporation flux in almost all land-use types: 50–64 % in forests, 61 % in grasslands, 72 % in croplands, and 58–65 % in shrublands. The exceptions are, logically, barren lands (17:BAR), snow/ice (16:ICE) and open waters (01:WAT).

Among the more vegetated land-use types, vegetation interception ratios are highest in forests (21–37 % of E), followed by croplands (17 %), and lowest in the sparsely vegetated land-use types: shrublands, savannahs, grasslands, wetlands, and urban lands (10–14 %). Floor interception values follow the pattern of vegetation interception. Thus, floor interception is generally higher than soil moisture evaporation in forests, whereas soil moisture evaporation equals or exceeds floor interception more often in shrublands and croplands.

Reported land-use specific evaporative partitioning in previous research is scarce at the global scale. Lawrence et al. (2007) do not report evaporative partitioning by land use (from simulation using Community Land Model version 3), but map figures indicate that their soil evaporation is higher and canopy interception is lower in savannahs, grasslands, and shrublands occupied areas compared to STEAM. Transpiration ratios of CLM3 are comparable with STEAM in forested and savannah areas, but are much lower (down to < 30 %) in the western US, India, southeastern China, and South Africa. Alton et al. (2009) report global mean transpiration ratios of 49–65 % in forests, 32–60 % in grassland, and 44–51 % in shrublands. The order of magnitude is similar to STEAM, but transpiration ratios for shrublands are lower. Schlesinger and Jasechko (2014) compiled satellite-based estimates from Mu et al. (2011) and arrived at 70 % transpiration in tropical forests, 55–67 % in other forests, and 57–62 % in grasslands. Choudhury et al. (1998) used a biophysical process-based model, and estimated transpiration ratio to amount to 56–77 % in three rainforest regions, 63–82 % in three savannah regions, and 37–82 % in seven cropland areas. Transpiration for river basins shown in the isotope study of Jasechko et al. (2013) show transpiration ratios above 70 % in grassland dominated areas in the western United States. van den Hoof et al. (2013) evaluated model performance against sites in temperate Europe, and reported transpiration rates of 47–78 % at eight forest sites, and 59–79 % at three grassland sites. Overall, STEAM falls well in the range of the reported evaporation partitioning ratios.

STEAM estimates the vegetation interception ratio as 18 % of rainfall in evergreen broadleaf forest, 17 % in deciduous broadleaf forest, and 18–20 % in needleleaf forest. In comparison, Miralles et al. (2010) arrived at higher canopy interception in coniferous (22 %) and deciduous forest (19 %) than in tropical forest (13 %) using satellite data analysis and literature review. Thus, interception ratios are comparable, except for tropical forest. In an interception scheme comparison study, Wang et al. (2007) found that taking rainfall type into account increased the performance and decreased interception in the tropics in comparison to the default CLM3 (Community Land Model version 3) interception scheme. Although STEAM uses an area reduction factor to scale interception, this may simply not be enough in the tropical, convective rainfall regimes. On the other hand, field studies have shown high interception ratios in the tropics. For example, Cuartas et al. (2007) reported 16.5 % for two years in Central Amazon, Franken et al. (1992) reported 19.8 % in Central Amazon, and Tobón Marin et al. (2000) reported 12–17 % in Colombian Amazon over four years. Interestingly, Cuartas et al. (2007) also showed that the differences in dry and normal years can differ substantially: 13.3 % in a normal year and 22.6 % in a dry year.

Sensitivity of STEAM evaporation partitioning to precipitation is analysed by a 5 % uniform reduction of precipitation, see Appendix D.

5.3 Runoff

STEAM estimates the mean annual global runoff as $43\,216\,\mathrm{km^3\,year^{-1}}$ ($325\,\mathrm{mm\,year^{-1}}$, 37 % of $\overline{P}$). Based on discharge data and simulated stream flow simulations, Dai and Trenberth (2002) estimated runoff to be $37\,288 \pm 662\,\mathrm{km^3\,year^{-1}}$ (35 % of $\overline{P}$, excl. Greenland and Antarctica). Syed et al. (2010) arrived at $36\,055\,\mathrm{km^3\,year^{-1}}$ based on the global ocean mass balance, Oki and Kanae (2006) reported $45\,500\,\mathrm{km^3\,year^{-1}}$ including groundwater runoff, and the GRDC composite runoff (GRDC-Comp) is about $38\,000\,\mathrm{km^3\,year^{-1}}$ (Fekete et al., 2000). Thus, the STEAM runoff estimate appears to be slightly higher than some of the previous estimates, but lies within the uncertainty range. Differences can partly be explained by the terrestrial area considered in the studies, as well as relatively high P applied (see Appendix D).

STEAM runoff was also compared to GRDC-Comp, GRDC-WBM, and ERA-I runoff data in 13 major river basins of the world, see Figs. 7 and 8a. The largest deviations for both STEAM and ERA-I from the GRDC-Comp runoff are found in the Congo and Nile river basins. However, because Congo precipitation and runoff estimates are particularly uncertain in general (Tshimanga, 2012), we can not evaluate our Congo evaporation estimate based on this specific comparison. As for the Nile river basin, STEAM uses a static land-use map that does not include seasonal variations in wetland size or presence of reservoirs. Since the Nile contains the Sudd, one of the largest wetlands in the world with a highly variable size, evaporation simulation is challenging in this region, even in fine resolution models including complex processes (Mohamed, 2005; Mohamed et al., 2007). In several of the northern river basins (e.g., the Mississippi, Mackenzie, and Danube), STEAM runoff is low in comparison to GRDC-Comp. There could be multiple reasons for this underestimation: our simplified snow simulation, our uniform parametrisation of land-use classes across climate zones or simply uncertainties in the forcing data. In support of the latter, the largest uncertainties in evaporation inferred from precipitation and runoff data occur mainly in the higher latitudes (Vinukollu et al., 2011).

Table 4 shows that the STEAM evaporation is close to the mean evaporation provided by the WaterMIP (Water Model Intercomparison Project) (Haddeland et al., 2011; Harding et al., 2011), while both the simulated runoff and the used precipitation forcing is substantially lower. In contrast, in the Lena river basin, STEAM runoff is in range while both evaporation and precipitation have a high bias. In the Amazon basin, the default STEAM simulation slightly overestimates runoff, but reducing precipitation forcing by 5 % (see the 95 %-P run in Fig. 7) brings runoff down to the level in GRDC-Comp. Also the comparison with WaterMIP indicates that high bias in Amazon precipitation translates into high runoff. This effect of precipitation reduction can also be noted in particularly the Brahmaputra–Ganges, Congo, and Nile river basins. This is not surprising, because precipitation uncertainties have been shown to translate almost entirely into uncertainty in runoff in wet regions, but not at all in arid regions (e.g., Fekete et al., 2004). The relative sensitivity of runoff and evaporation fluxes to precipitation is further accounted for in Appendix D.

The standard deviations between the multiyear mean runoffs in GRDC-Comp (which we here consider as the benchmark runoff) and the other runoffs (GRDC-WBM, ERA-I, and STEAM) are shown in Fig. 8b and c. Among the compared datasets, STEAM runoff deviates the most from GRDC-Comp when Congo is included and the least when Congo is excluded. Note also that omitting irrigation in STEAM increases the runoff deviation to GRDC-Comp, and that reducing precipitation decreases this deviation. Thus, the wet bias in ERA-I precipitation probably explains some of the runoff overestimations we notice in STEAM.

5.4 Irrigation

The simulated mean gross irrigation is $1970\,\mathrm{km^3\,year^{-1}}$, and the simulated mean increase in evaporation from irrigation is $1134\,\mathrm{km^3\,year^{-1}}$. The irrigation hotspots in especially India, south-eastern China, and the central US coincide well with where evaporation is enhanced by irrigation input. Our estimates are comparable to previous estimates. Gross irrigation was estimated at $2500\,\mathrm{km^3\,year^{-1}}$ by Döll and Siebert (2002), at $2353\,\mathrm{km^3\,year^{-1}}$ by Seckler et al. (1998), and at $1660\,\mathrm{km^3\,year^{-1}}$ by Rost et al. (2008). The latter study did, however, not take into account recharge to the groundwater. Evaporation contribution by irrigation was simulated at $1100\,\mathrm{km^3\,year^{-1}}$ by Döll and Siebert (2002). While higher evaporation contributions have also been reported in the literature, such as $2600\,\mathrm{km^3\,year^{-1}}$ by Gordon et al. (2005), they could possibly be explained by differences in methods and irrigation maps. Given the uncertainties, the modeling results are considered acceptable in terms of total amounts.

6 Results: temporal characteristics

6.1 Terrestrial time scales

The modelled global average time scale (Eq. 27) is 1.3 h for vegetation interception and 7.7 h for floor interception, but 42 days for soil moisture evaporation and 274 days for transpiration in areas with mean evaporation rates higher than $0.01\,\mathrm{mm\,d^{-1}}$. Evaporation rates from vegetation cover and floor are large compared to their respective stocks, resulting in small time scales for interception. In contrast, the stocks in the unsaturated zone are many times larger than the interception stocks, and cause the time scales of soil moisture evaporation and transpiration to extend from days and months. The use of an area reduction factor (see Eq. 21 and 22) leads to interception storage capacities that are smaller in the model than in reality, thus, presumably causing some underestimation of the interception time scales. Nevertheless, the robustness test (Table 5) shows that the magnitude of all evaporation time scales (except for transpiration) are relatively robust against uncertainties in storage capacities.

Figure 9 shows the spatial distribution of mean terrestrial residence time scales (i.e., stock divided by flux) of the partitioned evaporation fluxes (Eq. 27). We see that time scales are in general prolonged over the tropics, and over the cold northern latitudes. This finding is consistent with the transpiration response time scale provided by Scott et al. (1997). Over the tropics, evaporation rates are high, but the stocks are also relatively larger. The time scales of floor and soil moisture evaporation are extended in the tropics, because these fluxes there are suppressed by the relatively high vegetation interception and transpiration.

The temporal variation of the evaporation fluxes at different latitudes is displayed in Fig. 10. Seasonality is distinct for all evaporation fluxes, in particular for transpiration time scales. While the mean latitude transpiration time scale can extend to over 500 days in the mid-latitude winter, it falls well below 100 days in the summer.

Regions and seasons with extremely high transpiration time scales (>300 days) largely coincide with low transpiration in the north, whereas high transpiration rates coincide with intermediate or low time scales (<100 days). On the contrary, relatively high vegetation interception time scales seem positively correlated with high vegetation interception in the tropics, (compare Fig. 2 and 9). This difference can be explained by the limiting factor to evaporation. Transpiration time scales approach infinity as the stock is still wet, whereas vegetation interception time scale often approaches zero when vegetation interception is caused by depletion in vegetation interception stock rather than in evaporative demand. Thus, the high transpiration time scales in the north should be understood as the result of declining evaporative demand, whereas the high vegetation interception time scales in the tropics can be interpreted as the result of a steady and ample supply of precipitation to the vegetation interception stock.

The higher the interception ratios, the lower the evaporation time scales on land (also in consistency with e.g., Scott et al. (1995)), and the faster the overall feedback to the atmosphere. The regions that have a high vegetation interception ratio (Fig 5) coincide with the regions with low atmospheric moisture recycling length scales (van der Ent and Savenije, 2011). This suggests that tropical interception is very important for vegetation to maintain atmospheric moisture in the air, and could constitute a large portion of local recycling due to immediate feedback. However, moisture supplied to continents in general (van der Ent et al., 2010), the world's most important croplands (Bagley et al., 2012), or for rainfall dependent regions (Keys et al., 2012) also relies on remote evaporation sources, which could account for a large part of transpiration. For such cases, upwind modifications that result in changed transpiration rates (e.g., changes in vegetation species, rainwater harvesting practice, CO_2 concentrations) may play a larger role for downwind regions than changes in interception. A detailed investigation of the role of interception and transpiration for local and remote moisture recycling is performed in Part 2.

6.2 Evaporation partitioning in relation to time since precipitation

Figure 11 shows the mean latitudinal evaporation ratios by time since precipitation last occurred. Mean latitudinal transpiration ratio is up to 40 % during the wet time steps with precipitation, but can amount to up to 90 % after just a few dry 3 hour time steps. The largest increase in transpiration ratios with time since precipitation are seen in the cold northern latitudes, where moisture availability is expected to exceed evaporative demand. On the contrary, the vegetation interception ratio is high (up to approximately 60 %) during wet time steps, but falls drastically to almost no interception within 6 hours. Similarly to transpiration, soil moisture evaporation ratios generally increase with precipitation-free hours. However, the steepest increase in soil moisture evaporation ratios are found in the equatorial band where the total soil moisture evaporation is very low.

Table 5 shows that transpiration and soil moisture evaporation occur both during wet and dry conditions, whereas vegetation and floor interception evaporation occur almost exclusively during time steps with precipitation. The table shows that 31 % of all transpiration occurs during time steps that have endured more than one day of no precipitation, when no vegetation interception occur. Instead, 96 % of the vegetation interception occurs in a 3 hour time step with precipitation, whereas only 45 % of transpiration evaporates in such conditions. Noteworthy is also that these evaporation efficiency numbers (Eq. 29) are robust to changes in the evaporation partitioning: for example, the 96 % vegetation interception efficiency persists even when the vegetation interception ratio varies between 12 and 27 %. In other words, even with large differences in the evaporation ratio, interception is likely to occur almost exclusively within the wet period, whereas transpiration may have a substantial time lag between the moment water enters the soil and exits through a plant's stomata. In for example the field study of Farah et al. (2004), transpiration at a tropical woodland site continued for two months after rainfall. This also explains why transpiration dominates in the dry season and could have substantial effects on moisture recycling patterns (which will be analysed in Part 2). Furthermore, although a change in evaporation partitioning does not change the vegetation interception and transpiration efficiencies, it changes the total evaporation efficiency and the overall temporal distribution of evaporation.

7 Summary and conclusions

This paper developed and evaluated the global hydrological land-surface model STEAM, and used the model output to analyse the terrestrial temporal characteristics of different evaporation fluxes on land. STEAM is designed to 1) be tailored for coupling with the atmospheric moisture recycling model WAM-2layers, 2) be flexible for land-use change by land-use parametrisation and by including representation of features particularly important for evaporation (e.g., phenology and irrigation), 3) remain simple, transparent and computationally efficient, and 4) simulate evaporation and evaporation partitioning in line with current knowledge.

The ability of STEAM to simulate evaporation and evaporation partitioning realistically was evaluated by comparison with other modelling studies, global datasets, and reported values from field studies. STEAM's total terrestrial evaporation rate (73,900 $\text{km}^3\,\text{year}^{-1}$) is comparable with previous estimates – lower than reanalysis products, but higher than other land-surface models. Reasons for this include that we do not add water in data assimilation as in reanalysis, and compared to other land-surface models we use a relatively high precipitation input and also include irrigation and wetlands. Overall, STEAM simulates global evaporation partitioning within the range of previous estimates: 59 % transpiration, 21 % vegetation interception, 10 % floor interception, and 6 % soil moisture evaporation. The global mean transpiration ratio in STEAM is similar to or somewhat higher than other land-surface models, and in line with the recent literature compilation study of Schlesinger and Jasechko (2014). Vegetation interception ratios in forests are comparable with both the findings from a global satellite based estimate of interception (Miralles et al., 2010) and with reported values from field studies in the tropics. In agreement with previous studies (McNaughton and Jarvis, 1983; de Bruin and Jacobs, 1989; Teuling et al., 2010), STEAM also simulates higher transpiration ratios in short vegetation types than in forests.

Simplifications in STEAM include neglect of runoff routing, groundwater, and sublimation processes. Koster and Milly (1997) and Koster and P. Mahanama (2012) concluded among others that compatibility between runoff and evaporation formulations can be important due to interaction through soil moisture. Dry season evaporation might also be underestimated by the neglect of groundwater (Miguez-Macho and Fan, 2012) and hydraulic redistribution of soil water by roots (Lee et al., 2005). Crop simulations presently also do not follow sowing and harvesting dates. The neglect of sublimation can further cause underestimation of interception (Schlaepfer et al., 2014). Nevertheless, the model evaluation analyses and the sensitivity tests suggest that that the current model setup is a reasonable simplification for the research questions asked.

Our analyses show a striking difference in mean annual global time scales between the different evaporation fluxes: 95-434 days for transpiration, 42-46 days for soil moisture evaporation, 5.2-11.6 hours for floor interception, and 1.1-1.6 hours for vegetation interception. The time scales also vary greatly over the seasons and latitudes. Most transpiration occurs several hours or days after a rain event, whereas interception is immediate. We find that 31 % of all transpiration occurs in time steps that have endured more than one day without precipitation, when no vegetation interception occurs. Instead, 96 % of the vegetation interception occurs in a 3 hour time step with precipitation, whereas only 45 % of the transpiration occurs in such conditions. Uncertainties in parametrising storage capacities affect the evaporation partitioning ratios, but have a smaller effect on the relative differences in temporal characteristics. Only the transpiration time scales are significantly changed by changed storage capacity, but are still substantially different from the interception time scales. We note that high vegetation interception ratios coincide with high local evaporation recycling, which suggests that tropical interception may have an important role for vegetation to maintain atmospheric moisture in the air. This will be subject to further investigation in Part 2.

STEAM runs at the same temporal and spatial scale as the atmospheric moisture recycling model WAM-2layers, and can be used in both one and two-way coupling. One-way coupling, i.e., forcing WAM-2layers with STEAM output, is used in Part 2 to investigate the differences in moisture recycling between direct and delayed evaporation fluxes. Two-way coupling, i.e., feeding induced changes in precipitation from WAM-2layers back to STEAM, can be applied in later studies to investigate the effect of land-use change on moisture recycling. Although WAM-2layers does not simulate precipitation, such analyses are possible by assuming that changes in terrestrial evaporation proportionally alters the atmospheric moisture content or the precipitation with continental origin.

The importance of land use for the hydrological cycle, the climate, and the Earth system as a whole has been stressed in many studies (e.g., Feddema et al., 2005; Gordon et al., 2005; Rockström et al., 2009a). Thus, changes in evaporative partitioning following e.g., land-use change may have implications and provide answers for landscape resilience, drought development, and effects on remote fresh water resources. The differences in moisture recycling patterns between delayed and direct evaporation fluxes constitutes the case for investigation in Part 2 for the present day situation. Future research should also extend to land-use change scenario analysis to quantify and improve the assessment of land-use change effects on global fresh water resources.

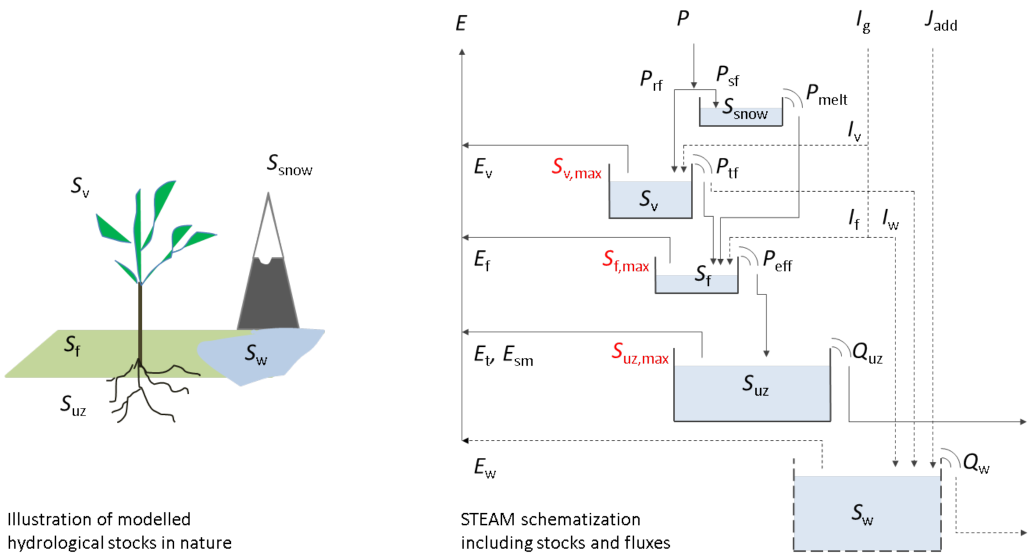

Fig. 1. Water fluxes and stocks in STEAM. Arrows indicate fluxes, and boxes indicate stocks. Dashed lines indicate fluxes and stocks that only exist for particular land-use types. Symbols are listed in Appendix A. A model description is offered in Sect. 2.

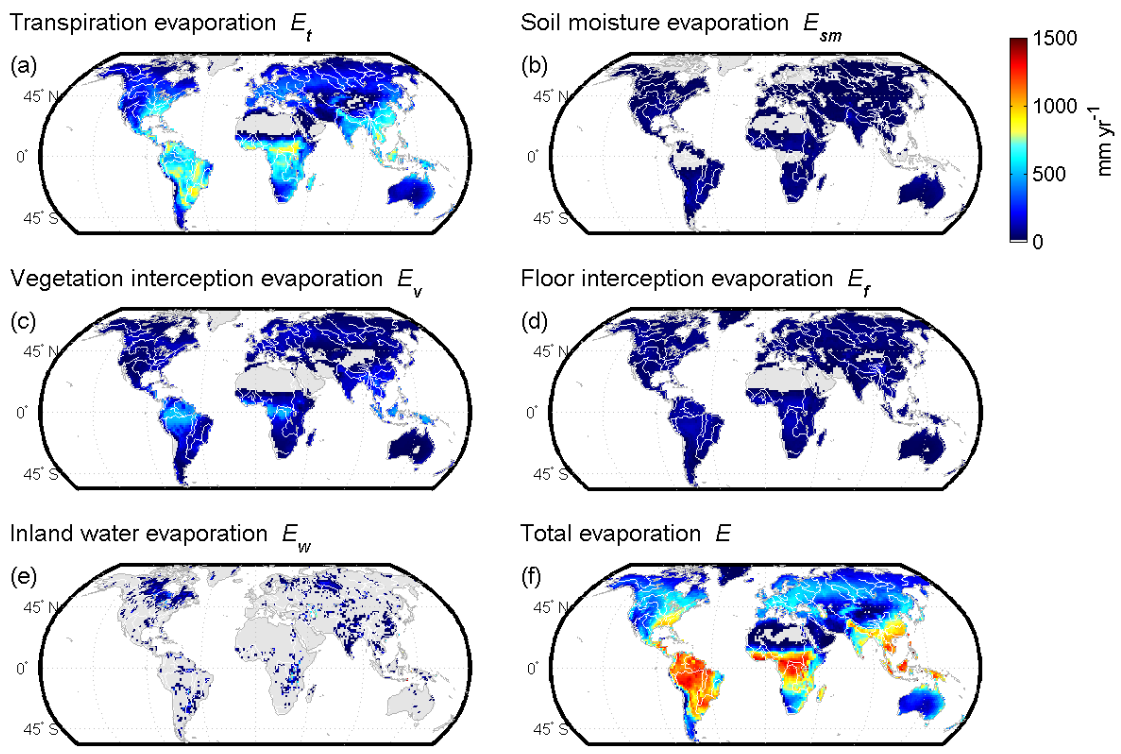

Fig. 2. Mean annual evaporation as estimated by STEAM (1999–2008). Grey indicates areas where the evaporative flux is zero. Results are discussed in Sect. 5.1 and 5.2.

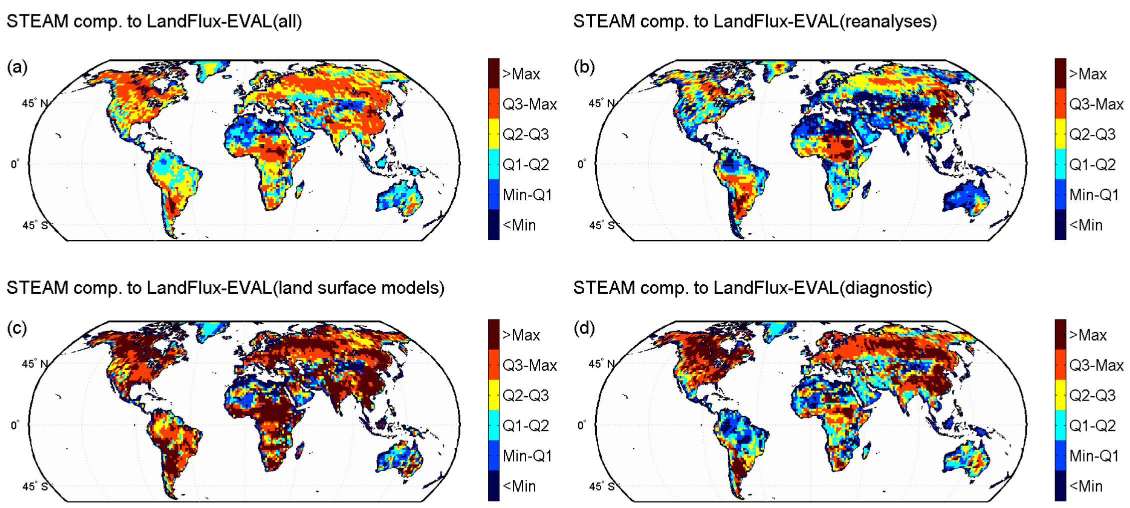

Fig. 3. Annual mean STEAM evaporation compared to the statistics (minimum, first quartile, median, third quartile, maximum) of the LandFlux-EVAL product (1989-2005) for **(a)** merged synthesis, **(b)** reanalyses, **(c)** land surface models, and **(d)** diagnostic datasets. Results are discussed Sect. 5.1.

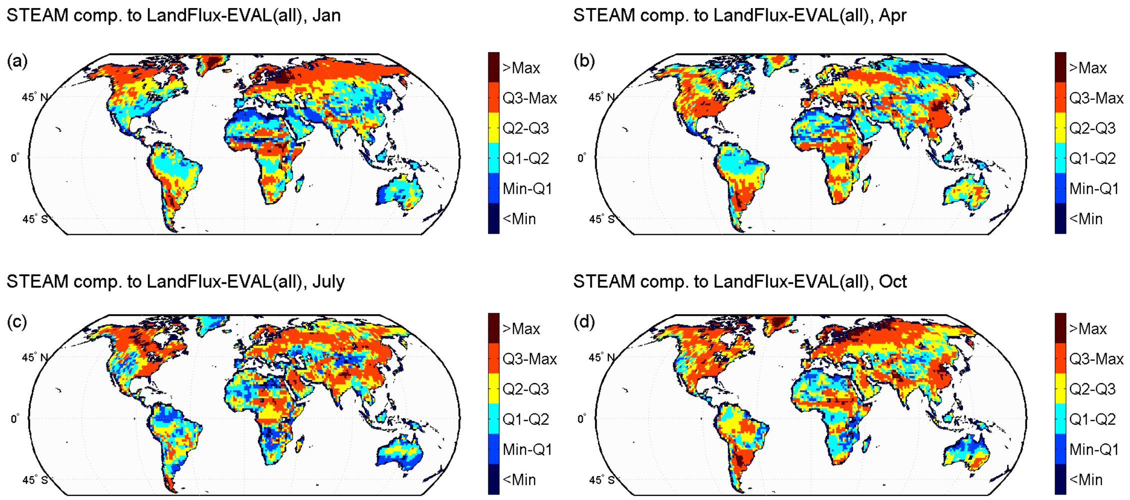

Fig. 4. Monthly mean STEAM evaporation compared to the statistics (minimum, first quartile, median, third quartile, maximum) of the merged synthesis LandFlux-EVAL product (1989-2005) for **(a)** January, **(b)** April, **(c)** July, and **(d)** October. Results are discussed Sect. 5.1.

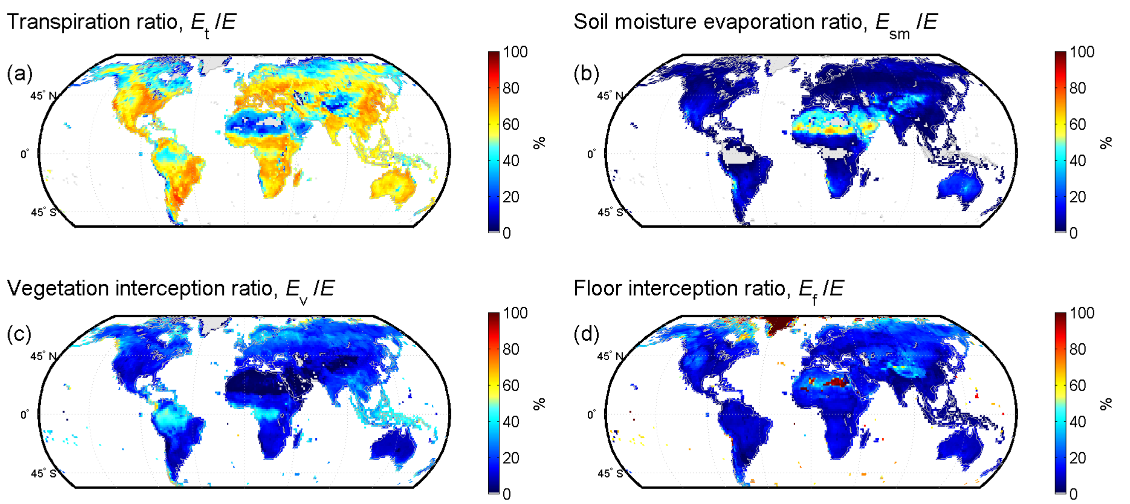

Fig. 5. Partitioned evaporation fluxes expressed as a percentage of total mean annual evaporation (1999–2008). Grey indicates areas where evaporation percentage is zero. Results are discussed in Sect. 5.2.

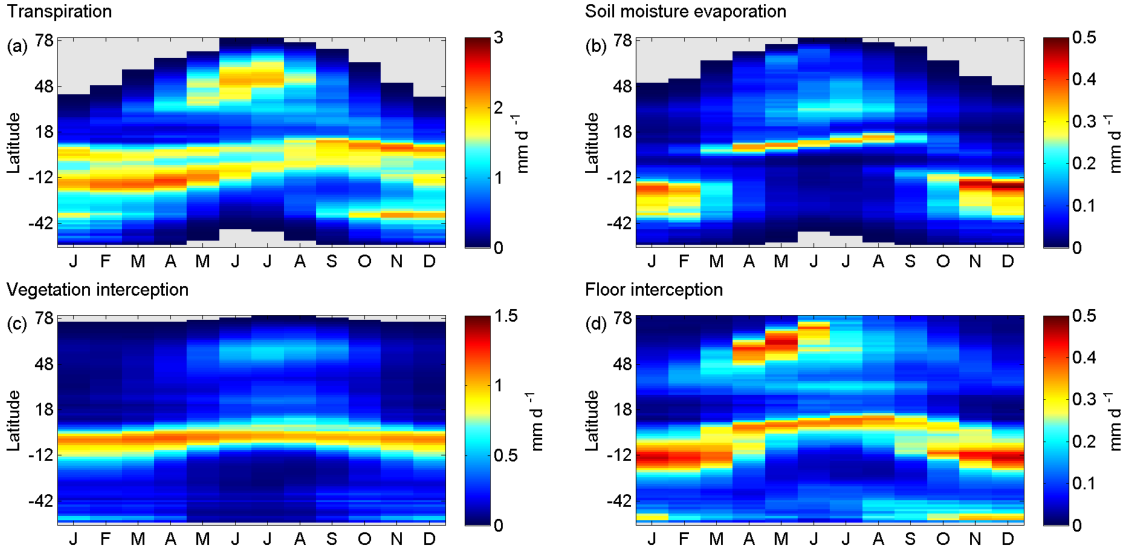

Fig. 6. Mean monthly evaporation as estimated by STEAM for different latitudes (1999-2008). Note that the scales are different for the different evaporation fluxes. Grey indicates where the evaporative flux is near zero. Results are discussed Sect. 5.2.

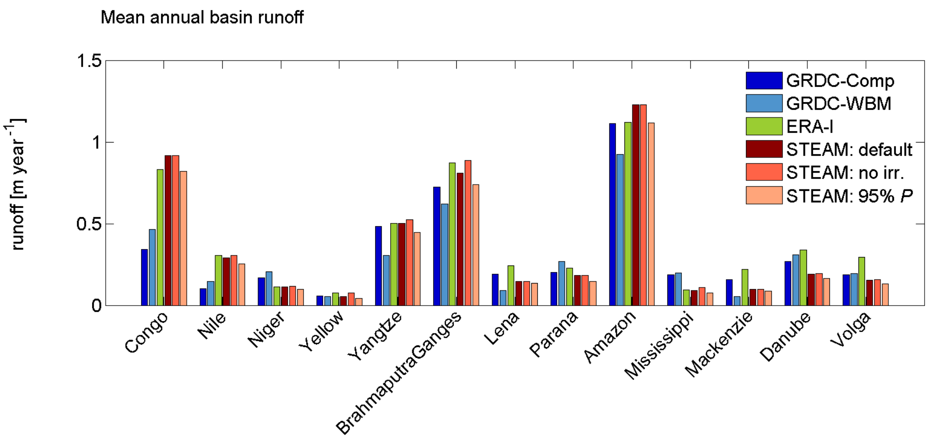

Fig. 7. Mean annual runoff of STEAM compared to other datasets (described in Sect. 3). GRDC-Comp (Global Runoff Data Centre composite runoff fields) is the GRDC-WBM (Water Balance Model) runoff corrected using inter-station discharge data. STEAM is run with three settings: with default settings (STEAM: default), with irrigation module switched off (STEAM: no irr) and with 5 % uniform in precipitation forcing (STEAM: 95 % P). STEAM runoff ($\overline{P} - \overline{E} - (\overline{\mathrm{d}S\mathrm{snow}/\mathrm{d}t})$) and ERA-I runoff are for the years 1999–2008. GRDC-Comp and GRDC-WBM represent longterm runoff. Results are discussed in Sect. 5.3.

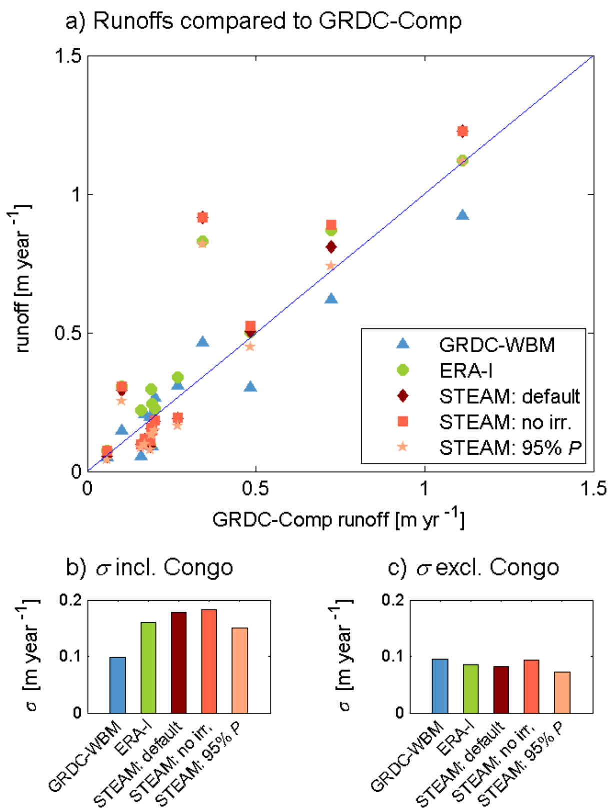

Fig. 8. Comparison between GRDC-Comp (which we consider the benchmark runoff) and the GRDC-WBM, ERA-I, and STEAM runoffs. **(a)** shows the 1 : 1 agreement line; **(b)** shows the standard deviations σ of GRDC-WBM, ERA-I, and STEAM river basin runoff to GRDC-Comp when Congo is included, and **(c)** shows the standard deviations when Congo is excluded. Results are discussed in Sect. 5.3.

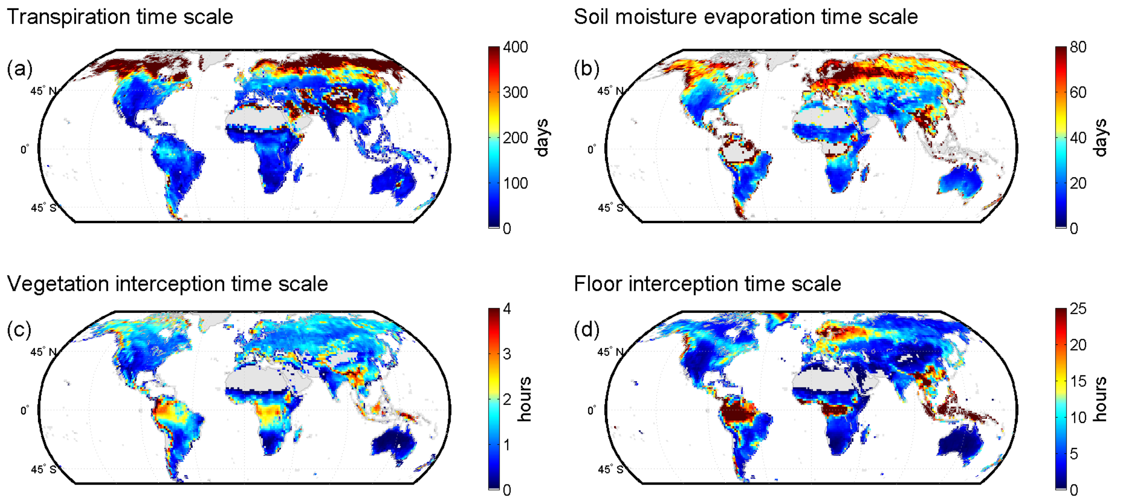

Fig. 9. Average surface time scales of different evaporation fluxes: **(a)** transpiration, **(b)** soil moisture evaporation, **(c)** vegetation interception, and **(d)** floor interception (1999–2008). Grey indicates grid cells with mean evaporation rates below 0.01 $\mathrm{mm\,d^{-1}}$. Note that the units are in hours for E_v and E_f, and in days for E_t and E_sm, see Eq. (27). Results are discussed in Sect. 6.1.

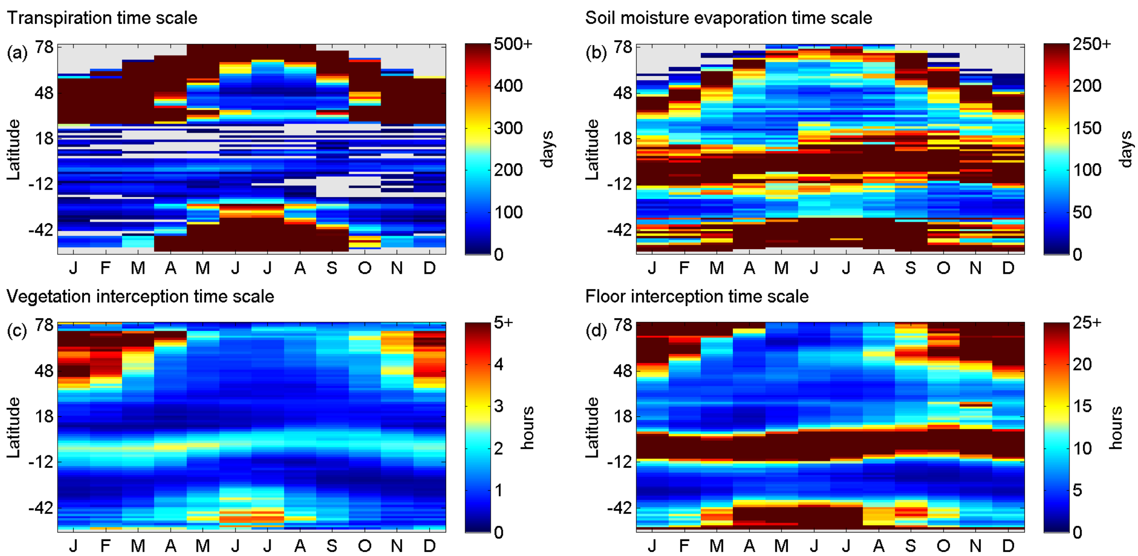

Fig. 10. Changes in terrestrial time scales (Eq. 27) over the year and different latitudes (1999-2008). Note that the units are in hours for E_v and E_f, and in days for E_t and E_sm. Grey indicates when time scale approaches infinity. Results are discussed in Sect. 6.1

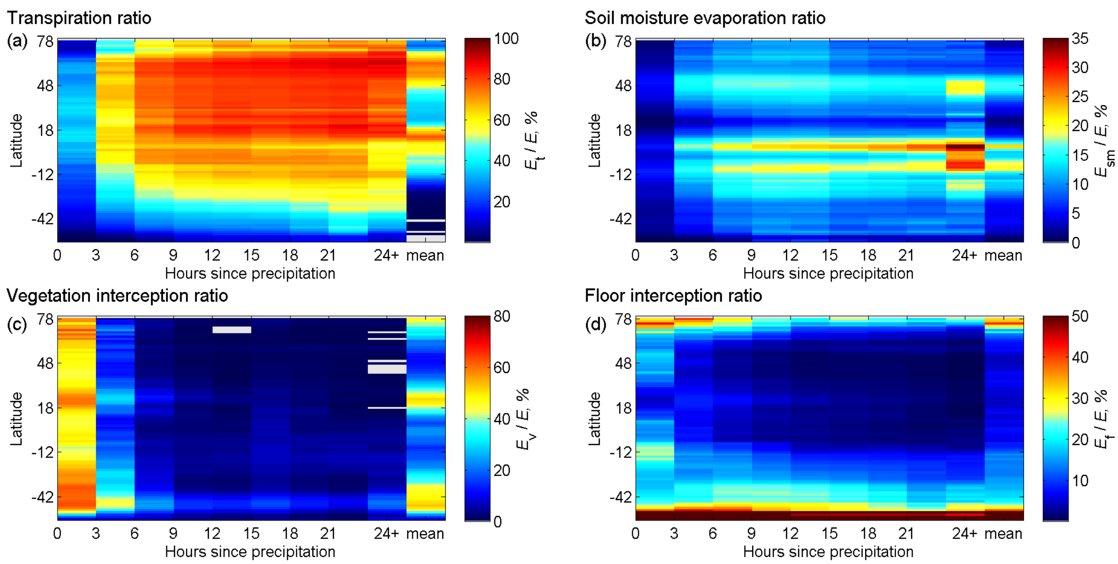

Fig. 11. Evaporation partitioning with time since precipitation over terrestrial latitudes (1999-2008). Results are discussed in Sect. 6.2.

Table 1. Evaporation and evaporation partitioning by land-use type, 1999–2008. Symbols are explained in Appendix A. Results are discussed in Sect. 5.1 and 5.2.

Land use	Area	P	E	E_v	E_f	E_t	E_sm	E_w	E_v	E_f	E_t	E_sm	E_w	E_v
Unit	1000 km^2	mm year^{-1}							% of E					% of P
01: WAT	1071	937	1147	0	0	0	0	1147	0	0	0	0	100	0
02: ENF	3224	853	496	155	73	248	20	0	31	15	50	4	0	18
03: EBF	13 541	2542	1208	452	92	652	13	0	37	8	54	1	0	18
04: DNF	1341	481	366	95	67	191	14	0	26	18	52	4	0	20
05: DBF	1350	1057	853	179	83	543	48	0	21	10	64	6	0	17
06: MXF	9349	958	604	158	80	345	21	0	26	13	57	4	0	16
07: CSH	99	554	499	54	57	324	64	0	11	11	65	13	0	10
08: OSH	21 207	432	281	38	44	162	37	0	14	16	58	13	0	9
09: WSA	10 585	1210	735	103	89	495	48	0	14	12	67	6	0	9
10: SAV	9904	1122	861	102	91	602	66	0	12	11	70	8	0	9
11: GRA	18 253	616	394	54	66	241	33	0	14	17	61	8	0	9
12: WET	1218	1151	957	114	26	297	8	513	12	3	31	1	54	10
13: CRP	(10 352–10 851)[a]	789	577	99	23	417	38	0	17	4	72	7	0	13
14: URB	454	991	465	46	42	256	120	0	10	9	55	26	0	5
15: MOS	(7790–7814)[a]	1262	779	165	79	509	25	0	21	10	65	3	0	13
16: ICE	2710	560	32	0	32	0	0	0	0	100	0	0	0	0
17: BAR	18 943	90	57	1	11	20	25	0	1	19	36	44	0	1
18: IRR	(1060–1195)[a]	727	1375	271	81	910	113	0	20	6	66	8	0	37
19: RIC	(175–570)[a]	1453	1458	242	7	547	4	659	17	0	37	0	45	17
Global	133 146	888	555	115	58	326	33	24	59	10	21	6	4	13

[a] Area varies because a monthly varying irrigation map is applied.

Table 2. Evaporation of lumped land-use types in comparison with other studies. Results are discussed in Sect. 5.1

	STEAM, Year 1999–2008		Gordon et al. (2005)		Schlesinger and Jasechko (2014) based on Mu et al. (2011)	Rockström et al. (1999)
	Area	Average E	Area	Average E	Average E	Average E
Unit	1000 km^2	[mm year^{-1}]	1000 km^2	[mm year^{-1}]	[mm year^{-1}]	[mm year^{-1}]
Forest[a]	28 805	875	46 665	660		
Evergreen needleleaf	3224	496	2134	510	458[e]	487[i]
Evergreen broadleaf	13 541	1208	16 278	1146	1076	1245
Deciduous needleleaf	1341	366		293–795[d]	458[e]	
Deciduous broadleaf	1350	853		293–795[d]	549[f]	729–792[d]
Mixed	9349	604	14 222	313		
Savannah	20 489	735–861[b]	19 562	556		416[j]/882/1267[k]
Shrubland	21 306	281–499[c]	18 649	227	302[g]	270[l]
Grassland	18 253	393	14 393	258	332–583[h]	410[m]

[a] Includes all forest types.
[b] Woody savannah (09:WSA) and savannah (10:SAV).
[c] Closed shrubland (07:CSH) and open shrubland (08:OSH).
[d] Deciduous forests in general.
[e] Temperate coniferous forest.
[f] Temperate deciduous forest.
[g] Mediterranean shrubland.
[h] Temperate and tropical grassland.
[i] Coniferous forest in general.
[j] Woody savannah.
[k] Wet savannah.
[l] Dry shrubland.
[m] Cool grassland.

Table 3. Overview of global evaporative partitioning estimates. Results are discussed in Sect. 5.2.

	E_{t}	E_{v}	$(E_{\mathrm{f}}+E_{\mathrm{sm}})$	Source
Unit		$\%$ of E		
Land-surface models				
STEAM	59	21	16	This study
JULES (with SiB or SPA scheme)	38–48			(Alton et al., 2009)
CLM3	44	17	39	(Lawrence et al., 2007)
LPJ	65			(Gerten et al., 2005)
A biophysical process-based model	52	20	28	(Choudhury et al., 1998)
Other methods				
Literature	61			(Schlesinger and Jasechko, 2014)
Isotope + literature	35–80			(Coenders-Gerrits et al., 2014)
Isotope + literature	80–90			(Jasechko et al., 2013)
GLEAM, satellite-based method	80	11	7	(Miralles et al., 2011)
Multimodel, GSWP2	48	16	36	(Dirmeyer et al., 2006)

Table 4. Comparison of STEAM output (1999–2008) with evaporation and runoff provided by the WaterMIP (Water Model Intercomparison Project) (1985–1999) (Haddeland et al., 2011; Harding et al., 2011). The ERA-I precipitation used to force STEAM and the WFD (Watch Forcing Data) precipitation used to force WaterMIP are also shown for each compared river basin. Results are discussed in Sect. 5.3.

	E_{STEAM}	E_{WaterMIP}			Q_{STEAM}	Q_{WaterMIP}			$P_{\text{ERA-I}}$	P_{WFD}
		Low	Mean	High		Low	Mean	High		
Unit	$\mathrm{mm\,year^{-1}}$									
Amazon	1154	1021	1195	1430	1228	815	1043	1207	2382	2243
Mississippi	595	492	642	747	93	167	269	418	692	909
Ganges/Brahmaputra	739	410	546	828	809	553	891	1038	1555	1447
Lena	319	172	230	283	148	103	151	211	487	385
Global	555	415	499	586	325	290	375	457	888	872

Table 5. Robustness to storage capacity parametrisation of STEAM, (global mean for 1999–2008). The subscript $_\mathrm{t}$ stands for transpiration, $_\mathrm{sm}$ for soil moisture evaporation, $_\mathrm{v}$ for vegetation interception, $_\mathrm{f}$ for floor interception, and $_\mathrm{uz}$ for unsaturated zone. Methods are described in Sect. 4.2.3 and results are discussed in Sect. 6.1 and 6.2.

	Default	Transpiration-plus	Interception-plus
Storage capacity			
$S_\mathrm{v,max}$	100 %	50 %	150 %
$S_\mathrm{f,max}$	100 %	50 %	150 %
$S_\mathrm{uz,max}$	100 %	120 %	80 %
Total evaporation	73,900 $\mathrm{km^3\,year^{-1}}$	73,200 $\mathrm{km^3\,year^{-1}}$	74,200 $\mathrm{km^3\,year^{-1}}$
Evaporation ratio			
E_t/E	59 %	64 %	54 %
E_sm/E	6 %	7 %	5 %
E_v/E	21 %	12 %	27 %
E_f/E	10 %	12 %	10 %
Time scales			
$\tau_\mathrm{ts,t}$	274 days	434 days	95 days
$\tau_\mathrm{ts,sm}$	42 days	43 days	46 days
$\tau_\mathrm{ts,v}$	1.3 hours	1.1 hours	1.6 hours
$\tau_\mathrm{ts,f}$	7.7 hours	5.2 hours	11.6 hours
Evaporation efficiency, $<$3 hours after precipitation[a]			
β_wet	58 %	56 %	60 %
$\beta_\mathrm{wet,t}$	45 %	46 %	43 %
$\beta_\mathrm{wet,sm}$	39 %	44 %	35 %
$\beta_\mathrm{wet,v}$	96 %	96 %	96 %
$\beta_\mathrm{wet,f}$	83 %	87 %	79 %
Evaporation efficiency, $>$24 hours without precipitation[b]			
β_dry	23 %	24 %	21 %
$\beta_\mathrm{dry,t}$	31 %	31 %	31 %
$\beta_\mathrm{dry,sm}$	32 %	29 %	34 %
$\beta_\mathrm{dry,v}$	1 %	1.2 %	0.8 %
$\beta_\mathrm{dry,f}$	3.9 %	2.8 %	5 %

[a] The evaporation efficiency is calculated for 3 hour time steps with precipitation.

[b] The evaporation efficiency is calculated for 3 hour time steps that have been without precipitation for more than 24 hours.

Appendix A

Notations

Symbols used in this paper are listed and defined in Table A1.

Table A1. List of symbols.

Symbol	Units	Description
α	–	Albedo
β	–	Evaporation efficiency, i.e., the portion of evaporation evaporated during certain conditions.
γ	$\mathrm{kPa\,K^{-1}}$	Psychrometric constant
Δn	h	Time step, 24 h
Δt	h	Time step, 3 h
δ	$\mathrm{kPa\,K^{-1}}$	Slope of the saturated vapour pressure curve
η_{clay}	%	Clay content of the top soil
Θ_{top}	–	Effective saturation of top soil
θ_{top}	–	Volumetric soil moisture content of top soil
$\theta_{\mathrm{top,\,sat}}$	–	Volumetric soil moisture content of top soil at saturation
$\theta_{\mathrm{top,\,res}}$	–	Volumetric soil moisture content of top soil at residual point
θ_{uz}	–	Volumetric soil moisture content of the unsaturated zone
$\theta_{\mathrm{uz,\,fc}}$	–	Volumetric soil moisture content at field capacity in the unsaturated zone
$\theta_{\mathrm{uz,\,wp}}$	–	Volumetric soil moisture content at wilting point
κ	–	Von Kármán constant, 0.41.
λ	$\mathrm{MJ\,kg^{-1}}$	Latent heat of vaporisation of water
ξ_{mw}	–	Ratio of the molecular weight of water vapour to that for dry air, 0.622.
ρ_{a}	$\mathrm{kg\,m^{-3}}$	Density of air.
ρ_{w}	$\mathrm{kg\,m^{-3}}$	Density of water
τ_{ts}	day	Mean terrestrial time scale
ϕ_{lu}	–	Land-use fraction
ϕ_{ow}	–	Open water fraction
ϕ_{vs}	–	Vegetation in soil fraction
ϕ_{vw}	–	Vegetation in water fraction
χ	h	Top soil moisture dry out time parameter
χ_{min}	h	Minimum top soil moisture dry out time parameter, 60 h.
C_p	$\mathrm{MJ\,kg^{-1}\,K^{-1}}$	Heat capacity of water at constant pressure, 1.01×10^{-3} $\mathrm{MJ\,kg^{-1}\,K^{-1}}$

Table A1. Continued.

Symbol	Units	Description
c_{AR}	–	Area reduction factor, 0.4
c_{D1}	–	Vapor pressure stress parameter, 3.
c_{D2}	–	Vapor pressure stress parameter, 0.1.
c_{R}	–	Radiation stress parameter, 100.
c_{sc}	–	Storage capacity factor, 0.2.
c_{uz}	–	Soil moisture stress parameter, 0.07
$D_{0.5}$	kPa	Vapour pressure deficit coefficient, 1.5 kPa
D_{a}	kPa	Vapour pressure deficit
d	m	Zero plane displacement
E	$\mathrm{m\,d^{-1}}$	Total evaporation
E_{f}	$\mathrm{m\,d^{-1}}$	Floor interception evaporation
$E_{\mathrm{f,\,lu,\,vs}}$	m $(\Delta t)^{-1}$	Land-use specific floor interception evaporation in ϕ_{vs}
E_{p}	m $(\Delta t)^{-1}$	Potential evaporation
$E_{\mathrm{p,\,day}}$	$\mathrm{m\,d^{-1}}$	Potential evaporation
E_{sm}	$\mathrm{m\,d^{-1}}$	Soil moisture evaporation
$E_{\mathrm{sm,\,lu,\,vs}}$	m $(\Delta t)^{-1}$	Land-use specific soil moisture evaporation in ϕ_{vs}
E_{t}	$\mathrm{m\,d^{-1}}$	Transpiration evaporation
$E_{\mathrm{t,\,lu,\,vs}}$	m $(\Delta t)^{-1}$	Land-use specific transpiration in ϕ_{vs}
$E_{\mathrm{t,\,lu,\,vw}}$	m $(\Delta t)^{-1}$	Land-use specific transpiration in ϕ_{vw}
E_{v}	$\mathrm{m\,d^{-1}}$	Vegetation interception evaporation
$E_{\mathrm{v,\,lu,\,vs}}$	m $(\Delta t)^{-1}$	Land-use specific vegetation interception evaporation in ϕ_{vs}
$E_{\mathrm{v,\,lu,\,vw}}$	m $(\Delta t)^{-1}$	Land-use specific vegetation interception evaporation in ϕ_{vw}
E_{w}	$\mathrm{m\,d^{-1}}$	Open water evaporation
$E_{\mathrm{w,\,lu,\,ow}}$	m $(\Delta t)^{-1}$	Land-use specific water evaporation in ϕ_{ow}
$E_{\mathrm{w,\,lu,\,vw}}$	m $(\Delta t)^{-1}$	Land-use specific open water evaporation in ϕ_{ow}
e_{a}	kPa	Actual vapor pressure
e_{s}	kPa	Saturated vapor pressure
G	$\mathrm{MJ\,m^{-2}\,d^{-1}}$	Ground heat flux
h	m	Plant height
h_{max}	m	Minimum plant height

Table A1. Continued.

Symbol	Units	Description
h_{min}	m	Maximum plant height
I_{f}	$\text{m}\,\text{d}^{-1}$	Irrigation applied to S_{f}
I_{g}	$\text{m}\,\text{d}^{-1}$	Gross irrigation
I_{req}	m $(\Delta t)^{-1}$	Irrigation requirement
I_{uz}	$\text{m}\,\text{d}^{-1}$	Irrigation applied to S_{uz}
I_{v}	$\text{m}\,\text{d}^{-1}$	Irrigation applied to S_{v}
i_{GS}	–	Growing Season Index
i_{LA}	$\text{m}^2\,\text{m}^{-2}$	Leaf Area Index
$i_{\text{LA,eff}}$	$\text{m}^2\,\text{m}^{-2}$	Effective Leaf Area Index
$i_{\text{LA,max}}$	$\text{m}^2\,\text{m}^{-2}$	Maximum Leaf Area Index
$i_{\text{LA,min}}$	$\text{m}^2\,\text{m}^{-2}$	Minimum Leaf Area Index
J_{add}	m $(\Delta t)^{-1}$	Water added in water stores to compensate for lack of horizontal flows
k	–	Function of r_{a} and r_{s}
N	s	Day length
N_{high}	s	Day length, higher sub-optimal threshold, assumed to be 39 600 s.
N_{low}	s	Day length, lower sub-optimal threshold, assumed to be 36 000 s.
P	$\text{m}\,\text{d}^{-1}$	Total precipitation
P_{eff}	$\text{m}\,\text{d}^{-1}$	Effective precipitation, (i.e., overflow from floor interception stock to unsaturated zone stock)
P_{melt}	$\text{m}\,\text{d}^{-1}$	Snowmelt
P_{rf}	m $(\Delta t)^{-1}$	Rainfall
P_{sf}	m $(\Delta t)^{-1}$	Snowfall
P_{tf}	m $(\Delta t)^{-1}$	Throughfall, (i.e., overflow from vegetation interception stock to floor interception stock)
p	kPa	atmospheric pressure
Q_{uz}	m $(\Delta t)^{-1}$	Outlow from S_{uz}
Q_{w}	m $(\Delta t)^{-1}$	Runoff from S_{w}
R_{net}	$\text{MJ}\,\text{m}^{-2}\,\text{d}^{-1}$	Net radiation
$R_{\text{net, lw}}$	$\text{MJ}\,\text{m}^{-2}\,\text{d}^{-1}$	Net long wave radiation
R_{sw}	$\text{MJ}\,\text{m}^{-2}\,\text{d}^{-1}$	Short wave radiation

Table A1. Continued.

Symbol	Units	Description
r_{a}	$\mathrm{d\,m^{-1}}$	Aerodynamic resistance
$r_{\mathrm{a,\,f}}$	$\mathrm{d\,m^{-1}}$	Floor aerodynamic resistance
$r_{\mathrm{a,\,v}}$	$\mathrm{d\,m^{-1}}$	Vegetation aerodynamic resistance
$r_{\mathrm{a,\,w}}$	$\mathrm{d\,m^{-1}}$	Open water aerodynamic resistance
r_{s}	$\mathrm{d\,m^{-1}}$	Surface resistance
$r_{\mathrm{s,\,sm}}$	$\mathrm{d\,m^{-1}}$	Surface soil moisture resistance
$r_{\mathrm{s,\,sm,\,min}}$	$\mathrm{d\,m^{-1}}$	Minimum surface soil moisture resistance
$r_{\mathrm{s,\,st}}$	$\mathrm{d\,m^{-1}}$	Surface stomatal resistance
$r_{\mathrm{s,\,st,\,min}}$	$\mathrm{d\,m^{-1}}$	Minimum surface stomatal resistance
S_{f}	m	Floor interception stock
$S_{\mathrm{f,\,lu}}$	m	Floor interception stock of a specific land-use type
$S_{\mathrm{f,\,max}}$	m	Floor interception storage capacity
S_{snow}	m	Snow stock
S_{uz}	m	Unsaturated stock
$S_{\mathrm{uz,\,lu}}$	m	Unsaturated stock of a specific land-use type
$S_{\mathrm{uz,\,max}}$	m	Unsaturated storage capacity
$S_{\mathrm{uz,\,sm}}$	m	Unsaturated stock available for soil moisture evaporation
$S_{\mathrm{uz,\,t}}$	m	Unsaturated stock available for transpiration
S_{v}	m	Vegetation interception stock
$S_{\mathrm{v,\,lu}}$	m	Vegetation interception stock of a specific land-use type
$S_{\mathrm{v,\,max}}$	m	Vegetation interception storage capacity
S_{w}	m	Water stock
$S_{\mathrm{w,\,lu}}$	m	Water stock of a specific land-use type

Table A1. Continued.

Symbol	Units	Description
T_{dew}	K	Dew point temperature
T_{mean}	K	Daily mean temperature
T_{min}	K	Daily minimum temperature
$T_{\text{min, high}}$	K	Daily minimum temperature, higher sub-optimal threshold, 278.15 K.
$T_{\text{min, low}}$	K	Daily minimum temperature, lower sub-optimal threshold, 271.15 K.
T_{opt}	K	Optimum photosynthesis temperature
u_{10}	$\mathrm{m\,d^{-1}}$	Wind speed at 10 m height
u_{200}	$\mathrm{m\,d^{-1}}$	Wind speed at 200 m height
u_{ref}	$\mathrm{m\,d^{-1}}$	Wind speed at reference height
y_{uz}	m	Depth of the unsaturated zone
y_{top}	m	Depth of the top soil
Z	m	Elevation
z_0	m	Aerodynamic roughness length
$z_{0,\text{f}}$	m	Roughness length of substrate floor
z_{10}	m	Height of wind speed u_{10}
z_{200}	m	Height of wind speed u_{200}
z_{ref}	m	Reference height

Appendix B

Model equations

B1 Input variables to the Penman–Monteith equation

The vapour pressure deficit D_a is defined as:

$$D_\mathrm{a} = e_\mathrm{s} - e_\mathrm{a}\left(T_\mathrm{dew}\right), \tag{B1}$$

where e_s [kPa] is the saturated vapour pressure at temperature T_mean [K] and estimated from the average of the saturated vapour pressures of the daily maximum and minimum temperature, e_a [kPa] is the vapour pressure of air at height z_ref [m], and T_dew [K] is the daily mean dew point temperature. Vapor pressure e_a is estimated from the formula below:

$$e_\mathrm{a}\left(T_\mathrm{dew}\right) = \frac{0.6108 {e_\mathrm{a}}^{17.27(T_\mathrm{dew}-273.15)}}{T_\mathrm{dew}-35.85}. \tag{B2}$$

For the estimation of e_s, T_dew was replaced by T_max or T_min. The latent heat of water vaporisation λ [$\mathrm{MJ\,kg^{-1}}$] is expressed as:

$$\lambda = 2.501 - 0.002361\left(T_\mathrm{mean} - 273.15\right). \tag{B3}$$

The gradient δ [$\mathrm{kPa\,K^{-1}}$] of the saturated vapour pressure function is given by

$$\delta = \frac{4098 \times e_\mathrm{s}}{237.3 + \left(T_\mathrm{mean} - 273.15\right)^2}. \tag{B4}$$

The psychrometric constant γ [$\mathrm{kPa\,K^{-1}}$] is

$$\gamma = \frac{C_p p}{\xi_\mathrm{mw}\lambda}, \tag{B5}$$

where p is the atmospheric pressure [kPa], and ξ_mw is the ratio of the molecular weight of water vapour to that for dry air [0.622].

Net radiation is calculated by:

$$R_\mathrm{net} = (1-\alpha)R_\mathrm{sw} - R_\mathrm{net,\,lw} \tag{B6}$$

where α is albedo, R_sw is the incoming shortwave radiation and $R_\mathrm{net,\,lw}$is the outgoing net longwave radiation. In reality, albedo varies with angle of reflection and the surface properties such as snow cover change and soil wetness. Here, we assume α to be fixed for each land-use type, see Table C1.

Daily ground heat flux G is derived from interpolating monthly ground heat flux G_{month} (Allen et al., 1998)

$$G_{month} = 0.07(\mathrm{T}_{month+1}\text{-}\mathrm{T}_{month-1}). \tag{B7}$$

There are three types of aerodynamic resistances used in STEAM: the aerodynamic vegetation resistance $r_\mathrm{a,\,v}$, the aerodynamic floor resistance $r_\mathrm{a,\,f}$, and the aerodynamic water resistance $r_\mathrm{a,\,w}$. They are expressed as follows (Shuttleworth, 2012):

$$r_\mathrm{a,\,v} = \frac{\ln\frac{z_\mathrm{ref}-d}{z_0}\ln\frac{z_\mathrm{ref}-d}{0.1z_0}}{u_\mathrm{ref,\,v}\kappa^2}, \tag{B8}$$

$$r_\mathrm{a,\,f} = \frac{\ln\frac{z_\mathrm{ref,\,f}}{z_\mathrm{0,f}}\ln\frac{z_\mathrm{ref,\,f}}{0.1z_\mathrm{0,f}}}{u_\mathrm{ref,\,f}\kappa^2}, \tag{B9}$$

$$r_\mathrm{a,\,w} = \frac{4.72\ln^2\frac{z_\mathrm{ref,\,w}}{z_\mathrm{0,f}}}{1+0.536u_\mathrm{ref,\,w}}, \tag{B10}$$

where z_ref is the reference height [m], z_0 is the aerodynamic roughness length [m], d is the zero-plane displacement height [m] and u_ref is the wind speed [$\mathrm{m\,d^{-1}}$] at z_ref. Wind speed u_ref is estimated from wind speed u_{10} given by ERA-I at $10\,\mathrm{m}$ z_{10} [m] under the assumption of a logarithmic wind profile and stable neutral atmospheric conditions:

$$u_\mathrm{ref,\,f} = u_{10}\frac{\ln\frac{z_\mathrm{ref,\,f}}{z_\mathrm{0,f}}}{\ln\frac{z_{10}}{z_\mathrm{0,f}}}, \tag{B11}$$

$$u_\mathrm{ref,\,w} = u_{10}\frac{\ln\frac{z_\mathrm{ref,\,w}}{z_\mathrm{0,f}}}{\ln\frac{z_{10}}{z_\mathrm{0,f}}}, \tag{B12}$$

where the reference height $z_\mathrm{ref,\,f}$ and $z_\mathrm{ref,\,w}$ are $2\,\mathrm{m}$ and $z_\mathrm{ref,\,v}$ is $2+h$ [m], with h being the plant height [m]. However, because some vegetation is higher than $10\,\mathrm{m}$, wind speed at $200\,\mathrm{m}$ is substituted into the formula to derive wind speeds at lower elevations:

$$u_\mathrm{ref,\,v} = u_{10}\frac{\ln\left(\frac{z_{200}}{z_0}\right)}{\ln\left(\frac{z_{10}}{z_0}\right)}\frac{\ln\left(\frac{z_\mathrm{ref,\,v}-d}{z_0}\right)}{\ln\left(\frac{z_{200}-d}{z_0}\right)}. \tag{B13}$$

The aerodynamic roughness length z_0 [m] is estimated from:

$$z_0 = \begin{cases} z_\mathrm{0,f} + 0.29h\sqrt{0.2i_\mathrm{LA}} & i_\mathrm{LA} \le 1 \\ 0.3h\left(1-d/h\right) & i_\mathrm{LA} > 1 \end{cases}. \tag{B14}$$

Zero plane displacement d is estimated from h [m] and i_LA [$\mathrm{m^2\,m^{-2}}$]

$$d = 1.1h\ln\left[1+\left(0.2i_\mathrm{LA}\right)^{0.25}\right], \tag{B15}$$

$$h = h_\mathrm{min} + \left(h_\mathrm{max} - h_\mathrm{min}\right)i_\mathrm{LA}/i_\mathrm{LA,max}. \tag{B16}$$

B2 Surface stomatal resistance

Surface resistance applies only to transpiration and soil moisture evaporation, since interception and open water evaporation occur without resistance. The surface stomatal resistance $r_\mathrm{s,\,st}$ of vegetation is simulated by the Jarvis–Stewart equation (Stewart, 1988), taking into account of solar radiation, vapour pressure deficit, optimum temperature, and soil moisture stress:

$$r_\mathrm{s,\,st} = \frac{r_\mathrm{s,\,st,\,min}}{i_\mathrm{LA,eff}f\left(R_\mathrm{sw}\right)f\left(D_\mathrm{a}\right)f\left(T_\mathrm{mean}\right)f\left(\theta_\mathrm{uz}\right)}, \tag{B17}$$

where $r_{\text{s, st, min}}$ is the minimum surface stomatal resistance dependent on land-use type and specified in the land-use look-up table (Table C1), $i_{\text{LA,eff}}$ is the effective leaf area index (unit leaf area per unit ground area that is actively participating in transpiration) and f are the four stress functions for incoming shortwave radiation R_{sw} in W m^{-2}, vapour pressure deficit D_{a}, mean daily temperature T_{mean} and soil moisture θ_{uz} (Stewart, 1988). Effective leaf area index $i_{\text{LA,eff}}$ is adapted from Allen et al. (2006) and Zhou et al. (2006) as:

$$i_{\text{LA,eff}} = \frac{i_{\text{LA}}}{0.2 i_{\text{LA}} + 1}. \tag{B18}$$

The stress functions vary between 0 and 1. The stress function of soil moisture $f(\theta_{\text{uz}})$ is the same as in Eq. (19). The other stress functions as follows (Jarvis, 1976; Zhou et al., 2006; Matsumoto et al., 2008):

$$f\left(R_{\text{sw}}\right) = R_{\text{sw}}\left(1 + c_{\text{R}}/1000\right)\left(c_{\text{R}} + R_{\text{sw}}\right)^{-1}, \tag{B19}$$

$$f\left(D_{\text{a}}\right) = \left[1 + \left(D_{\text{a}}/D_{\ 0.5}\right)^{c_{\text{D1}}}\right]^{-1}\left(1 - c_{\text{D2}}\right) + c_{\text{D2}}, \tag{B20}$$

$$f\left(T_{\text{mean}}\right) = \begin{cases} 0 & T_{\text{mean}} < 273.15 \\ 1 - T_{\text{opt}}{}^{-2}\left(T_{\text{mean}} - T_{\text{opt}}\right)^2 & \left(T_{\text{mean}} > T_{\text{opt}} + 1\right) \\ & \quad \cup \left(273.15 \leq T_{\text{mean}} < T_{\text{opt}} - 1\right), \\ 1 & T_{\text{opt}} - 1 \leq T_{\text{mean}} \leq T_{\text{opt}} + 1 \end{cases} \tag{B21}$$

where c_{R} is the radiation stress parameter fixed at 100 (Zhou et al., 2006), $D_{0.5}$ is the vapour pressure deficit halfway between 1 and c_{D2} set at 1.5 kPa, c_{D1} is the first vapour pressure parameter set at 3, and c_{D2} is the second vapour pressure stress parameter set at 0.1 (Matsumoto et al., 2008). Optimum temperature T_{opt} [K] is based on elevation a.s.l. Z [m] and latitude ω [rad] (Cui et al., 2012):

$$T_{\text{opt}} = 302.45 - 0.003\left(Z - |\omega|\right). \tag{B22}$$

Graphical representations of the stress functions are presented in Fig. B1. Under unfavourable conditions where at least one of the stress functions equals zero, $r_{\text{s, st}}$ is assumed to be $0.58\,\text{d}\,\text{m}^{-1}$ ($50\,000\,\text{s}\,\text{m}^{-1}$), corresponding to the molecular diffusivity of water vapour through leaf cuticula (Tourula and Heikinheimo, 1998). If i_{LA} is zero, no transpiration is allowed.

Appendix C

Primary land-use parameters

The parameters used to describe land use include maximum and minimum leaf area index $i_{\mathrm{LA,max}}$ and $i_{\mathrm{LA,min}}$, maximum and minimum plant height h_{max} and h_{min}, depth of the unsaturated zone (or rather active rooting depth) y_{uz}, albedo α, minimum stomatal resistance $r_{\mathrm{s,\,st,\,min}}$ and floor roughness $z_{0,\mathrm{f}}$. Land-use parameters considered include those used in other large-scale land-surface or hydrological models (Federer et al., 1996; van den Hurk et al., 2000; van den Hurk, 2003; Zhou et al., 2006; Bastiaanssen et al., 2012), and studies of specific land-use properties (Scurlock et al., 2001; Zeng, 2001; Breuer et al., 2003; Kleidon, 2004). The range of parameters in the literature can sometimes be significant and contradictory, due to discrepancies in scale, parameter definitions, and methods of parameter estimation. The choice of land-use parameters is therefore not simply taken as a mean from the literature values investigated, but rather based on the preservation of the internal consistency of STEAM, manual calibration and priority for literature values with higher relevance. In addition, some land-use types are assumed to contain water, either as water below vegetation or as open water. The land-use parameters used in the model are shown in Table C1, and the parametrisation of water fractions are presented in Table C2.

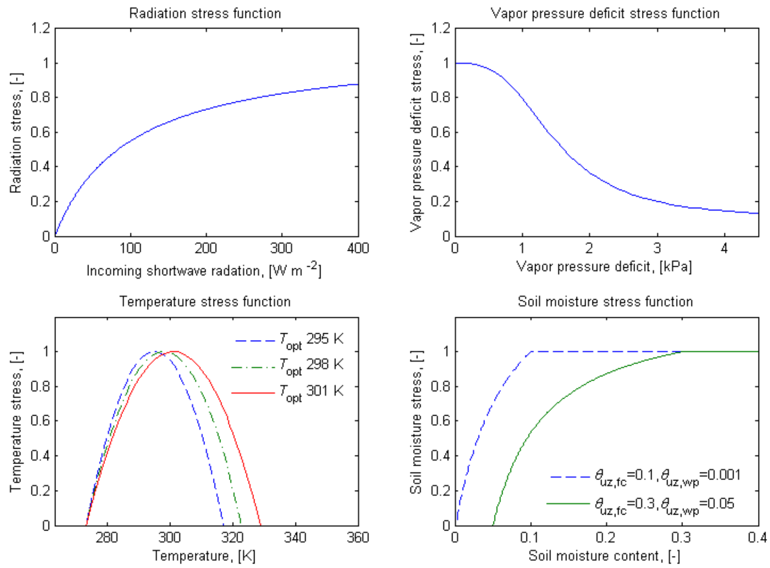

Fig. B1. Stress functions used in the Jarvis–Stewart equation (See Eq. B16.).

Table C1. Land-use parameters used in STEAM. For model description, see Sect. 2.

Land-use class	$i_{\text{LA,max}}$	$i_{\text{LA,min}}$	y_{uz}	α	h_{max}	h_{min}	$z_{0,\text{f}}$	$r_{\text{s, st, min}}$
Unit	–	–	m	–	m	m	m	$\text{s m}^{-1\text{a}}$
01: WAT (Water)	0	0	0	0.08	0	0	0.00137	0
02: ENF (Evergreen needleleaf forest)	5.5	2	2	0.15	17	17	0.02	300
03: EBF (Evergreen broadleaf forest)	5.5	2	2	0.18	30	30	0.02	200
04: DNF (Deciduous needleleaf forest)	5	1	2	0.18	17	17	0.02	300
05: DBF (Deciduous broadleaf forest)	5.5	1	2	0.18	25	25	0.02	200
06: MXF (Mixed forest)	5	1	2	0.18	20	20	0.02	250
07: CSH (Closed shrubland)	1.5	0.5	2	0.2	1.5	1.5	0.02	200
08: OSH (Open shrubland)	1.5	0.5	2	0.2	1	1	0.02	200
09: WSA (Woody savannah)	2	0.5	2	0.2	0.8	0.8	0.02	150
10: SAV (Savannah)	2	0.5	3.5	0.2	0.8	0.1	0.02	150
11: GRA (Grassland)	2	0.5	1.5	0.2	0.8	0.05	0.01	150
12: WET (Permanent wetland)	4	1	1.5	0.15	1	0.05	0.01	150
13: CRP (Cropland, rainfed)	3.5	0.5	1.5	0.2	0.8	0.05	0.005	150
14: URB (Urban and built-up)	1	0.1	0.5	0.18	0.8	0	0.001	250
15: MOS (Crop/natural mosaic)	3.5	0.5	1.5	0.2	0.8	0.1	0.005	150
16: ICE (Snow/ice)	0	0	0	0.7	0	0	0.001	0
17: BAR (Barren land)	0.1	0.01	1.5	0.25	0.8	0	0.001	200
18: IRR (Irrigated crop, excl. rice)	3.5	3.5	0.5	0.2	0.8	0.8	0.005	150
19: RIC (Irrigated rice paddies)	3.5	3.5	0.5	0.2	0.8	0.8	0.005	150

[a] The unit for $r_{\text{s, st, min}}$ is d m^{-1} throughout the paper, and only given as s m^{-1} in this table to facilitate comparison with other studies.

Table C2. Fractions of vegetation in soil ϕ_{vs}, vegetation in water ϕ_{vw}, and open water ϕ_{ow} by land-use type. Related equations are described in Sect. 2.2.

Land-use type	ϕ_{vs}	ϕ_{vw}	ϕ_{ow}
12:WET	$1/3$	$1/3$	$1/3$
19:RIC	$1/10$	$9/10$	0
01:WAT	0	0	1
Other	1	0	0

Appendix D

Sensitivity to precipitation

We perform a sensitivity check against precipitation because STEAM is forced by ERA-I precipitation reanalyses data, which is higher than several other satellite and/or gauge-based precipitation datasets. For the 1999–2008, the mean global ERA-I precipitation is $118\,236\,\mathrm{km}^3\,\mathrm{year}^{-1}$ for a land area of $133\,146\,465\,\mathrm{km}^2$. Other reported terrestrial precipitation values include $111\,000\,\mathrm{km}^3\,\mathrm{year}^{-1}$ (Oki and Kanae, 2006), $109\,500\,\mathrm{km}^3\,\mathrm{year}^{-1}$ from CRU, $111\,200\,\mathrm{km}^3\,\mathrm{year}^{-1}$ from PREC/L, and $112\,600\,\mathrm{km}^3\,\mathrm{year}^{-1}$ from GPCP (Trenberth et al., 2007).

Table D1 provides an overview of the sensitivity of runoff and evaporation fluxes to a uniform $5\,\%$ reduction in precipitation. A number of observations can be noted. First, the mean annual STEAM runoff is clearly more sensitive ($-10.95\,\%$) to precipitation reduction compared to evaporation ($-1.78\,\%$). Second, among the evaporation fluxes, soil moisture evaporation ($-2.95\,\%$) and transpiration ($-2.32\,\%$) respond most strongly, whereas the vegetation ($-0.89\,\%$) and floor interception ($-0.65\,\%$) evaporation fluxes reduce only marginally. This is logical, because interception stocks are already small and depend more on rainfall frequency than on rainfall amount. Third, the increase in open water evaporation ($+0.25\,\%$) is small, and can be explained by decreases in vegetation interception that translated into increases in available energy for water evaporation in wetlands and rice paddies. Fourth, the relative reduction in snow accumulation ($-14.63\,\%$) is high since snow melt is unchanged. Last, the global mean evaporative partitioning is changed only insignificantly towards lower transpiration ratio.

The sensitivity of transpiration is highest over the US, Australia, the subtropical South America and Africa, and other areas that at least during part of the years are water constrained. In the wet tropics, transpiration rates do not react to precipitation reductions. Vegetation interception experiences an insignificant relative decrease, which is highest in the north and highest in the tropics. This is probably caused by a combination of lower original interception rates in the boreal forests, and the relatively higher dependence on high rainfall frequency in the tropical forests.

This uniform perturbation of precipitation forcing indicates that STEAM evaporation is much less sensitive to precipitation than runoff. This can be explained by the fact that evaporation is constrained by potential evaporation, which relates to other factors than just precipitation. In wet regions where soil moisture is close to saturation, any excess precipitation would more likely lead to increase in runoff rather than evaporation. The sensitivity of runoff to precipitation data is also reported in the literature (e.g., Fekete et al., 2004; Materia et al., 2010) and supports the view that runoff comparisons will not accurately describe how well land-surface models estimate evaporation when precipitation is uncertain.

Table D1. Overview of the sensitivity of runoff, evaporation, and model snow accumulation to uniform reduction in precipitation quantity, (global mean for 1999–2008).

Flux	Default		5 % reduction in P		Change
	$\mathrm{km^3\,year^{-1}}$	% E	$\mathrm{km^3\,year^{-1}}$	% E	%
P	118 236	–	112 324	–	-5
Q	43 216	–	38 762	–	-10.3
E	73 933	100	72 644	100	-1.74
E_t	43 376	58.7	42 392	58.4	-2.27
E_v	15 288	20.7	15 152	20.9	-0.89
E_f	7706	10.4	7,657	10.5	-0.64
E_sm	4335	5.9	4207	5.8	-2.95
E_w	3228	4.4	3236	4.5	$+0.25$
$\mathrm{d}S_\mathrm{snow}/\mathrm{d}t$	1087	–	918	–	-15.5

Acknowledgements. L. Wang-Erlandsson and L. J. Gordon carried out this research by funding from the Swedish Research Council (Vetenskapsrådet). R. J. van der Ent and H. H. G. Savenije were funded by the research program Division for Earth and Life Sciences (ALW), which is financed by the Netherlands Organization for Scientific Research (NWO). We thank Wim Bastiaanssen, Jianzhi Dong, Johan Rockström, Patrick Keys, Jens Heinke, and Bart van den Hurk for valuable discussions during the model development. We would also like to thank the five anonymous reviewers for constructive comments on the manuscript.

References

Allen, R. G., Pereira, L. S., Raes, D., and Smith, M.: Crop evapotranspiration - Guidelines for computing crop water requirements - FAO Irrigation and drainage paper 56, Tech. rep., FAO - Food and Agriculture Organization of the United Nations, Rome, http://www.fao.org/docrep/x0490e/x0490e00.htm#Contents, 1998.

Allen, R. G., Pruitt, W. O., Wright, J. L., Howell, T. a., Ventura, F., Snyder, R., Itenfisu, D., Steduto, P., Berengena, J., Yrisarry, J. B., Smith, M., Pereira, L. S., Raes, D., Perrier, A., Alves, I., Walter, I., and Elliott, R.: A recommendation on standardized surface resistance for hourly calculation of reference ETo by the FAO56 Penman-Monteith method, Agricultural Water Management, 81, 1–22, doi:10.1016/j.agwat.2005.03.007, 2006.

Alton, P., Fisher, R., Los, S., and Williams, M.: Simulations of global evapotranspiration using semiempirical and mechanistic schemes of plant hydrology, Global Biogeochemical Cycles, 23, GB4032, doi:10.1029/2009GB003540, 2009.

Bagley, J. E., Desai, A. R., West, P. C., and Foley, J. A.: A Simple, Minimal Parameter Model for Predicting the Influence of Changing Land Cover on the Land–Atmosphere System?, Earth Interactions, 15, 1–32, doi:10.1175/2011EI394.1, 2011.

Bagley, J. E., Desai, A. R., Dirmeyer, P. A., and Foley, J. A.: Effects of land cover change on moisture availability and potential crop yield in the world's breadbaskets, Environmental Research Letters, 7, 014 009, doi:10.1088/1748-9326/7/1/014009, http://stacks.iop.org/1748-9326/7/i=1/a=014009?key=crossref.8f355b32de15c6b453f166d026d7f844, 2012.

Balsamo, G., Pappenberger, F., Dutra, E., Viterbo, P., and van den Hurk, B. J. J. M.: A revised land hydrology in the ECMWF model: a step towards daily water flux prediction in a fully-closed water cycle, Hydrological Processes, 25, 1046–1054, doi:10.1002/hyp.7808, 2011.

Bastiaanssen, W. G. M., Cheema, M. J. M., Immerzeel, W. W., Miltenburg, I. J., and Pelgrum, H.: The surface energy balance and actual evapotranspiration of the transboundary Indus Basin estimated from satellite measurements and the ETLook model, Water Resources Research, 48, W11 512, doi:10.1029/2011WR010482, 2012.

Breuer, L., Eckhardt, K., and Frede, H.-G.: Plant parameter values for models in temperate climates, Ecological Modelling, 169, 237–293, doi:10.1016/S0304-3800(03)00274-6, 2003.

Canadell, J., Jackson, R. B., Ehleringer, J. B., Mooney, H. a., Sala, O. E., and Schulze, E.-D.: Maximum rooting depth of vegetation types at the global scale, Oecologia, 108, 583–595, doi:10.1007/BF00329030, http://link.springer.com/10.1007/BF00329030, 1996.

Chen, B., Coops, N. C., Fu, D., Margolis, H. A., Amiro, B. D., Barr, A. G., Black, T. A., Arain, M. A., Bourque, C. P.-A., Flanagan, L. B., Lafleur, P. M., McCaughey, J. H., and Wofsy, S. C.: Assessing eddy-covariance flux tower location bias across the Fluxnet-Canada Research Network based on remote sensing and footprint modelling, Agricultural and Forest Meteorology, 151, 87–100, doi:10.1016/j.agrformet.2010.09.005, 2011.

Choudhury, B. J., DiGirolamo, N. E., Susskind, J., Darnell, W. L., Gupta, S. K., and Asrar, G.: A biophysical process-based estimate of global land surface evaporation using satellite and ancillary data II. Regional and global patterns of seasonal and annual variations, Journal of Hydrology, 205, 186–204, doi:10.1016/S0022-1694(97)00149-2, 1998.

Coenders-Gerrits, A. M. J., van der Ent, R. J., Bogaard, T. A., Wang-Erlandsson, L., Hrachowitz, M., and Savenije, H. H. G.: Uncertainties in transpiration estimates, Nature, 506, E1–E2, doi:10.1038/nature12925, 2014.

Crutzen, P. J.: Geology of mankind., Nature, 415, 23, doi:10.1038/415023a, 2002.

Cuartas, L. A., Tomasella, J., Nobre, A. D., Hodnett, M. G., Waterloo, M. J., and Múnera, J. C.: Interception water-partitioning dynamics for a pristine rainforest in Central Amazonia: Marked differences between normal and dry years, Agricultural and Forest Meteorology, 145, 69–83, doi:10.1016/j.agrformet.2007.04.008, 2007.

Cui, Y. P., Liu, J. Y., Hu, Y. F., Bing, L. F., Tao, F. L., and Wang, J. B.: Estimating and Analyzing the Optimum Temperature for Vegetation Growth in China (In Chinese), Journal of Natural Resources, 27, 281–292, 2012.

Czikowsky, M. J. and Fitzjarrald, D. R.: Detecting rainfall interception in an Amazonian rain forest with eddy flux measurements, Journal of Hydrology, 377, 92–105, doi:10.1016/j.jhydrol.2009.08.002, http://www.sciencedirect.com/science/article/pii/S0022169409004855, 2009.

Dai, A. and Trenberth, K. E.: Estimates of freshwater discharge from continents: Latitudinal and seasonal variations, Journal of hydrometeorology, 3, 660–687, doi:10.1175/1525-7541(2002)003<0660:EOFDFC>2.0.CO;2, 2002.

de Bruin, H. A. R. and Jacobs, C. M.: Forests and regional-scale processes, Biological Sciences, 324, 393–406, 1989.

de Jong, S. M. and Jetten, V. G.: Estimating spatial patterns of rainfall interception from remotely sensed vegetation indices and spectral mixture analysis, International Journal of Geographical Information Science, 21, 529–545, doi:10.1080/13658810601064884, 2007.

Dee, D., Uppala, S., Simmons, A. J., Berrisford, P., Poli, P., Kobayashi, S., Andrae, U., Balmaseda, M., Balsamo, G., Bauer, P., Bechtold, P., Beljaars, A. C. M., van de Berg, L., Bidlot, J., Bormann, N., Delsol, C., Dragani, R., Fuentes, M., Geer, A., Haimberger, L., Healy, S., Hersbach, H., Hólm, E., Isaksen, L., Kå llberg, P., Köhler, M., Matricardi, M., McNally, A., Monge-Sanz, B., Morcrette, J.-J., Park, B.-K., Peubey, C., de Rosnay, P., Tavolato, C., Thépaut, J.-N., and Vitart, F.: The ERA-Interim reanalysis: configuration and performance of the data assimilation system, Quarterly Journal of the Royal Meteorological Society, 137, 553–597, doi:10.1002/qj.828, 2011.

Delworth, T. and Manabe, S.: The influence of potential evaporation on the variabilities of simulated soil wetness and climate, Journal of Climate, 1, 523–547, http://journals.ametsoc.org/doi/abs/

10.1175/1520-0442(1988)001⟨0523:TIOPEO⟩2.0.CO;2, 1988.

Dirmeyer, P. A., Gao, X., Zhao, M., Guo, Z., Oki, T., and Hanasaki, N.: GSWP-2: Multimodel Analysis and Implications for Our Perception of the Land Surface, Bulletin of the American Meteorological Society, 87, 1381–1397, doi:10.1175/BAMS-87-10-1381, 2006.

Döll, P. and Lehner, B.: Validation of a new global 30-min drainage direction map, Journal of Hydrology, 258, 214–231, doi:10.1016/S0022-1694(01)00565-0, 2002.

Döll, P. and Siebert, S.: Global modeling of irrigation water requirements, Water Resources Research, 38, 8–1–8–10, doi:10.1029/2001WR000355, 2002.

Dore, M. H. I.: Climate change and changes in global precipitation patterns: what do we know?, Environment international, 31, 1167–81, doi:10.1016/j.envint.2005.03.004, 2005.

FAO/IIASA/ISRIC/ISSCAS/JRC: Harmonized World Soil Database (version 1.2), 2012.

Farah, H., Bastiaanssen, W., and Feddes, R.: Evaluation of the temporal variability of the evaporative fraction in a tropical watershed, International Journal of Applied Earth Observation and Geoinformation, 5, 129–140, doi:10.1016/j.jag.2004.01.003, 2004.

Feddema, J. J., Oleson, K. W., Bonan, G. B., Mearns, L. O., Buja, L. E., Meehl, G. A., and Washington, W. M.: The importance of land-cover change in simulating future climates, Science, 310, 1674–1678, doi:10.1126/science.1118160, 2005.

Feddes, R. A., Hoff, H., Bruen, M., Dawson, T., de Rosnay, P., Dirmeyer, P. A., Jackson, R. B., Kabat, P., Kleidon, A., Lilly, A., and Pitman, A. J.: Modeling Root Water Uptake in Hydrological and Climate Models, Bulletin of the American Meteorological Society, 82, 2797–2809, doi:10.1175/1520-0477(2001)082<2797:MRWUIH>2.3.CO;2, 2001.

Federer, C., Vörösmarty, C., and Fekete, B.: Intercomparison of methods for calculating potential evaporation in regional and global water balance models, Water Resources Research, 32, 2315–2321, doi:10.1029/96WR00801, 1996.

Fekete, B., Vörösmarty, C., Roads, J., and Willmott, C.: Uncertainties in precipitation and their impacts on runoff estimates, Journal of Climate, 17, 294–304, doi:10.1175/1520-0442(2004)017<0294:UIPATI>2.0.CO;2, 2004.

Fekete, B. M., Vörösmarty, C. J., and Grabs, W.: Global Composite Runoff Fields Based on Observed River Discharge and Simulated Water Balances, Tech. rep., Global Runoff Data Centre, Federal Insititute of Hydrology, Koblenz, 2000.

Franken, W., Leopoldo, P. R., Matsui, E., and Ribeiro, M. D. N. G.: Estudo da interceptação da água de chuva na coberta florestal Amazônica do tipo terra firme, Acta Amazonica, 12, 327–331, 1992.

Friedl, M. a., Sulla-Menashe, D., Tan, B., Schneider, A., Ramankutty, N., Sibley, A., and Huang, X.: MODIS Collection 5 global land cover: Algorithm refinements and characterization of new datasets, Remote Sensing of Environment, 114, 168–182, doi:10.1016/j.rse.2009.08.016, http://linkinghub.elsevier.com/retrieve/pii/S0034425709002673, 2010.

Gao, H., Hrachowitz, M., Fenicia, F., Gharari, S., and Savenije, H. H. G.: Testing the realism of a topography driven model (FLEX-Topo) in the nested catchments of the Upper Heihe, China, Hydrology and Earth System Sciences Discussions, 10, 12 663–12 716, doi:10.5194/hessd-10-12663-2013, 2013.

Gerrits, a. M. J., Savenije, H. H. G., Veling, E. J. M., and Pfister, L.: Analytical derivation of the Budyko curve based on rainfall characteristics and a simple evaporation model, Water Resources Research, 45, 1–15, doi:10.1029/2008WR007308, 2009.

Gerrits, a. M. J., Pfister, L., and Savenije, H. H. G.: Spatial and temporal variability of canopy and forest floor interception in a beech forest, Hydrological Processes, 24, 3011–3025, doi:10.1002/hyp.7712, 2010.

Gerten, D., Hoff, H., Bondeau, A., Lucht, W., Smith, P., and Zaehle, S.: Contemporary "green" water flows: Simulations with a dynamic global vegetation and water balance model, Physics and Chemistry of the Earth, Parts A/B/C, 30, 334–338, doi:10.1016/j.pce.2005.06.002, 2005.

Glarner, H.: Length of Day and Twilight, http://herbert.gandraxa.com/length_of_day.xml, 2006.

Gordon, L. J., Steffen, W., Jönsson, B. F., Folke, C., Falkenmark, M., and Johannessen, A. s.: Human modification of global water vapor flows from the land surface, PNAS, 102, 7612–7617, doi:10.1073/pnas.0500208102, 2005.

Haddeland, I., Clark, D. B., Franssen, W., Ludwig, F., Voß, F., Arnell, N. W., Bertrand, N., Best, M., Folwell, S., Gerten, D., Gomes, S., Gosling, S. N., Hagemann, S., Hanasaki, N., Harding, R., Heinke, J., Kabat, P., Koirala, S., Oki, T., Polcher, J., Stacke, T., Viterbo, P., Weedon, G. P., and Yeh, P.: Multimodel Estimate of the Global Terrestrial Water Balance: Setup and First Results, Journal of Hydrometeorology, 12, 869–884, doi:10.1175/2011JHM1324.1, http://journals.ametsoc.org/doi/abs/10.1175/2011JHM1324.1, 2011.

Harding, R., Best, M., Blyth, E., Hagemann, S., Kabat, P., Tallaksen, L. M., Warnaars, T., Wiberg, D., Weedon, G. P., van Lanen, H., Ludwig, F., and Haddeland, I.: WATCH: Current Knowledge of the Terrestrial Global Water Cycle, Journal of Hydrometeorology, 12, 1149–1156, doi:10.1175/JHM-D-11-024.1, 2011.

Herwitz, S. R.: Interception storage capacities of tropical rainforest canopy trees, Journal of Hydrology, 77, 237–252, doi:10.1016/0022-1694(85)90209-4, 1985.

Jackson, R. B., Canadell, J., Ehleringer, J. R., Mooney, H. A., Sala, O. E., and Schulze, E. D.: A global analysis of root distributions for terrestrial biomes, Oecologia, 108, 389–411, doi:10.1007/BF00333714, 1996.

Jarvis, P.: The interpretation of the variations in leaf water potential and stomatal conductance found in canopies in the field, Philosophical Transactions of the Royal Society of London, 273, 1976.

Jasechko, S., Sharp, Z. D., Gibson, J. J., Birks, S. J., Yi, Y., and Fawcett, P. J.: Terrestrial water fluxes dominated by transpiration, Nature, 496, 347–50, doi:10.1038/nature11983, 2013.

Jasechko, S., Sharp, Z. D., Gibson, J. J., Birks, S. J., Yi, Y., and Fawcett, P. J.: Jasechko et al. reply., Nature, 506, E2–3, doi:10.1038/nature12926, 2014.

Jiménez, C., Prigent, C., Mueller, B., Seneviratne, S. I., McCabe, M. F., Wood, E. F., Rossow, W. B., Balsamo, G., Betts, A. K., Dirmeyer, P. A., Fisher, J. B., Jung, M., Kanamitsu, M., Reichle, R. H., Reichstein, M., Rodell, M., Sheffield, J., Tu, K., and Wang, K.: Global intercomparison of 12 land surface heat flux estimates, Journal of Geophysical Research, 116, 1–27, doi:10.1029/2010JD014545, 2011.

Jolly, W. M., Nemani, R., and Running, S. W.: A generalized, bioclimatic index to predict foliar phenology in response to climate, Global Change Biology, 11, 619–632, doi:10.1111/j.1365-

2486.2005.00930.x, 2005.

Jung, M., Reichstein, M., Ciais, P., Seneviratne, S. I., Sheffield, J., Goulden, M. L., Bonan, G. B., Cescatti, A., Chen, J., de Jeu, R., Dolman, A., Eugster, W., Gerten, D., Gianelle, D., Gobron, N., Heinke, J., Kimball, J., Law, B. E., Montagnani, L., Mu, Q., Mueller, B., Oleson, K., Papale, D., Richardson, A. D., Roupsard, O., Running, S., Tomelleri, E., Viovy, N., Weber, U., Williams, C., Wood, E., Zaehle, S., and Zhang, K.: Recent decline in the global land evapotranspiration trend due to limited moisture supply, Nature, advance on, 951–4, doi:10.1038/nature09396, 2010.

Keys, P. W., van der Ent, R. J., Gordon, L. J., Hoff, H., Nikoli, R., and Savenije, H. H. G.: Analyzing precipitationsheds to understand the vulnerability of rainfall dependent regions, Biogeosciences, 9, 733–746, doi:10.5194/bg-9-733-2012, 2012.

Kleidon, A.: Global Datasets of Rooting Zone Depth Inferred from Inverse Methods, Journal of Climate, 17, 2714–2722, doi:10.1175/1520-0442(2004)017<2714:GDORZD>2.0.CO;2, http://journals.ametsoc.org/doi/abs/10.1175/1520-0442(2004)017⟨2714:GDORZD⟩2.0.CO;2, 2004.

Kleidon, A. and Heimann, M.: Assessing the role of deep rooted vegetation in the climate system with model simulations: mechanism, comparison to observations and implications for Amazonian deforestation, Climate Dynamics, 16, 183–199, doi:10.1007/s003820050012, 2000.

Koster, R. and Milly, P.: The interplay between transpiration and runoff formulations in land surface schemes used with atmospheric models, Journal of Climate, 10, 1578–1591, doi:10.1175/1520-0442(1997)010%3C1578:TIBTAR%3E2.0.CO;2, 1997.

Koster, R. D. and P. Mahanama, S. P.: Land Surface Controls on Hydroclimatic Means and Variability, Journal of Hydrometeorology, 13, 1604–1620, doi:10.1175/JHM-D-12-050.1, 2012.

Koster, R. D. and Suarez, M. J.: The influence of land surface moisture retention on precipitation statistics, Journal of Climate, 9, 2551–2567, doi:10.1175/1520-0442(1996)009<2551:TIOLSM>2.0.CO;2, 1996.

Lawrence, D. M., Thornton, P. E., Oleson, K. W., and Bonan, G. B.: The Partitioning of Evapotranspiration into Transpiration, Soil Evaporation, and Canopy Evaporation in a GCM: Impacts on Land–Atmosphere Interaction, Journal of Hydrometeorology, 8, 862–880, doi:10.1175/JHM596.1, 2007.

Lee, J.-E., Oliveira, R. S., Dawson, T. E., and Fung, I.: Root functioning modifies seasonal climate., Proceedings of the National Academy of Sciences of the United States of America, 102, 17 576–81, doi:10.1073/pnas.0508785102, 2005.

Liu, Y., Hiyama, T., Yasunari, T., and Tanaka, H.: A nonparametric approach to estimating terrestrial evaporation: Validation in eddy covariance sites, Agricultural and Forest Meteorology, 157, 49–59, doi:10.1016/j.agrformet.2012.01.012, 2012.

Lo, M.-h. and Famiglietti, J. S.: Irrigation in California ' s Central Valley strengthens the southwestern U . S . water cycle, Geophysical Research Letters, 40, doi:10.1002/GRL.50108, 2013.

Lohmann, D. and Wood, E. F.: Timescales of land surface evapotranspiration response in the PILPS phase 2(c), Global and Planetary Change, 38, 81–91, doi:10.1016/S0921-8181(03)00007-9, 2003.

Materia, S., Dirmeyer, P. A., Guo, Z., Alessandri, A., and Navarra, A.: The Sensitivity of Simulated River Discharge to Land Surface Representation and Meteorological Forcings, Journal of Hydrometeorology, 11, 334–351, doi:10.1175/2009JHM1162.1, 2010.

Matsumoto, K., Ohta, T., Nakai, T., Kuwada, T., Daikoku, K., Iida, S., Yabuki, H., Kononov, A. V., van der Molen, M. K., Kodama, Y., Maximov, T. C., Dolman, A. J., and Hattori, S.: Responses of surface conductance to forest environments in the Far East, Agricultural and Forest Meteorology, 148, 1926–1940, doi:10.1016/j.agrformet.2008.09.009, http://linkinghub.elsevier.com/retrieve/pii/S0168192308002505, 2008.

McNaughton, K. and Jarvis, P.: Predicting effects of vegetation changes on transpiration and evaporation, in: Water deficits and plant growth, edited by Kozlowski, T., pp. 1–47, Academic Press, New York, vol. 7 edn., 1983.

Miguez-Macho, G. and Fan, Y.: The role of groundwater in the Amazon water cycle: 2. Influence on seasonal soil moisture and evapotranspiration, Journal of Geophysical Research, 117, D15 114, doi:10.1029/2012JD017540, 2012.

Miralles, D. G., Gash, J. H., Holmes, T. R. H., de Jeu, R. a. M., and Dolman, A.: Global canopy interception from satellite observations, Journal of Geophysical Research, 115, 1–8, doi:10.1029/2009JD013530, 2010.

Miralles, D. G., De Jeu, R. a. M., Gash, J. H., Holmes, T. R. H., and Dolman, a. J.: Magnitude and variability of land evaporation and its components at the global scale, Hydrology and Earth System Sciences, 15, 967–981, doi:10.5194/hess-15-967-2011, 2011.

Miralles, D. G., van den Berg, M. J., Gash, J. H., Parinussa, R. M., de Jeu, R. A. M., Beck, H. E., Holmes, T. R. H., Jiménez, C., Verhoest, N. E. C., Dorigo, W. A., Teuling, A. J., and Johannes Dolman, A.: El Niño–La Niña cycle and recent trends in continental evaporation, Nature Climate Change, 4, 122–126, doi:10.1038/nclimate2068, 2013.

Mohamed, Y. A.: Impact of the Sudd wetland on the Nile hydroclimatology, Water Resources Research, 41, W08 420, doi:10.1029/2004WR003792, 2005.

Mohamed, Y. A., van den Hurk, B. J. J. M., and Savenije, H. H. G.: Moisture recycling over the Nile basin, in: Reducing the Vulnerability of Societies to Water Related Risks at the Basin Scale (Proceedings of the third International Symposium on Integrated Water Resources Management, Bochum, Germany), September 2006, pp. 18–23, IAHS Publ.317, http://www.knmi.nl/publications/fulltexts/iahs_mohamed_etal.pdf, 2007.

Monteith, J. L.: Evaporation and environment, in: Symp Soc Exp Biol, vol. 19, chap. The State, pp. 205–234, Cambridge University Press, Swansea, 1965.

Mu, Q., Zhao, M., and Running, S. W.: Improvements to a MODIS global terrestrial evapotranspiration algorithm, Remote Sensing of Environment, 115, 1781–1800, doi:10.1016/j.rse.2011.02.019, 2011.

Mueller, B., Hirschi, M., Jimenez, C., Ciais, P., Dirmeyer, P. A., Dolman, A. J., Fisher, J. B., Jung, M., Ludwig, F., Maignan, F., Miralles, D. G., McCabe, M. F., Reichstein, M., Sheffield, J., Wang, K., Wood, E. F., Zhang, Y., and Seneviratne, S. I.: Benchmark products for land evapotranspiration: LandFlux-EVAL multi-data set synthesis, Hydrology and Earth System Sciences, 17, 3707–3720, doi:10.5194/hess-17-3707-2013, 2013.

Oki, T. and Kanae, S.: Global hydrological cycles and world water resources., Science, 313, 1068–72, doi:10.1126/science.1128845, 2006.

Pellarin, T., Louvet, S., Gruhier, C., Quantin, G., and Legout, C.: A simple and effective method for correcting soil moisture and precipitation estimates using AMSR-E measurements, Remote Sensing of Environment, 136, 28–36, doi:10.1016/j.rse.2013.04.011, 2013.

Portmann, F. T., Siebert, S., and Döll, P.: MIRCA2000—Global monthly irrigated and rainfed crop areas around the year 2000: A new high-resolution data set for agricultural and hydrological modeling, Global Biogeochemical Cycles, 24, 1–24, doi:10.1029/2008GB003435, 2010.

Rockström, J., Gordon, L. J., Folke, C., Falkenmark, M., and Engwall, M.: Linkages among water vapor flows, food production, and terrestrial ecosystem services, Conservation Ecology, 3, 5, http://www.ecologyandsociety.org/vol3/iss2/art5/, 1999.

Rockström, J., Falkenmark, M., Karlberg, L., Hoff, H., Rost, S., and Gerten, D.: Future water availability for global food production: The potential of green water for increasing resilience to global change, Water Resources Research, 45, W00A12, doi:10.1029/2007WR006767, 2009a.

Rockström, J., Steffen, W., Noone, K., Persson, A., Chapin Iii, F. S., Lambin, E. F., Lenton, T. M., Scheffer, M., Folke, C., Schellnhuber, H. J., Nykvist, B., de Wit, C. A., Hughes, T., van der Leeuw, S., Rodhe, H., Sörlin, S., Snyder, P. K., Costanza, R., Svedin, U., Falkenmark, M., Karlberg, L., Corell, R. W., Fabry, V. J., Hansen, J., Walker, B., Liverman, D., Richardson, K., Crutzen, P., and Foley, J. A.: Planetary boundaries: Exploring the safe operating space for humanity, Ecology and Society, 14, 2009b.

Rohwer, J., Gerten, D., and Lucht, W.: Development of functional irrigation types for improved global crop modelling, Tech. Rep. 104, Potsdam Institute for Climate Impact Research, Potsdam, 2007.

Rost, S., Gerten, D., and Heyder, U.: Human alterations of the terrestrial water cycle through land management, Advances in Geosciences, 18, 43–50, doi:10.5194/adgeo-18-43-2008, http://www.gwsp.org/fileadmin/downloads/Rost-AdvGeo.pdf, 2008.

Savenije, H. H. G.: The importance of interception and why we should delete the term evapotranspiration from our vocabulary, Hydrological Processes, 18, 1507–1511, doi:10.1002/hyp.5563, 2004.

Saxton, K. E. and Rawls, W. J.: Soil Water Characteristic Estimates by Texture and Organic Matter for Hydrologic Solutions, Soil Science Society of America Journal, 70, 1569, doi:10.2136/sssaj2005.0117, 2006.

Schlaepfer, D. R., Ewers, B. E., Shuman, B. N., Williams, D. G., Frank, J. M., Massman, W. J., and Lauenroth, W. K.: Terrestrial water fluxes dominated by transpiration: Comment, Ecosphere, 5, art61, doi:10.1890/ES13-00391.1, 2014.

Schlesinger, W. H. and Jasechko, S.: Transpiration in the global water cycle, Agricultural and Forest Meteorology, 189-190, 115–117, doi:10.1016/j.agrformet.2014.01.011, 2014.

Scott, R., Koster, R. D., Entekhabi, D., and Suarez, M. J.: Effect of a canopy interception reservoir on hydrological persistence in a general circulation model, Journal of Climate, 8, 1917–1922, http://www.scopus.com/inward/record.url?eid=2-s2.0-0029478704&partnerID=tZOtx3y1, 1995.

Scott, R., Entekhabi, D., Koster, R., and Suarez, M.: Timescales of land surface evapotranspiration response, Journal of climate, 10, 559–566, doi:10.1175/1520-0442(1997)010<0559:TOLSER>2.0.CO;2, 1997.

Scurlock, J. M. O., Asner, G. P., and Gower, S. T.: Worldwide Historical Estimates of Leaf Area Index , 1932-2000, Tech. Rep. December, Oak Ridge National Laboratory, Tennessee, http://web.ornl.gov/~webworks/cppr/y2002/rpt/112600.pdf, 2001.

Seckler, D., Amarasinghe, U., Molden, D., de Silva, R., and Barker, R.: World Water Demand and Supply, 1990 to 2025: Scenarios and Issues, Tech. rep., International Water Management Institute (IWMI), Colombo, Sri Lanka, 1998.

Serafini, V. V. and Sud, Y. C.: The time scale of the soil hydrology using a simple water budget model, Journal of Climatology, 7, 585–591, doi:10.1002/joc.3370070606, 1987.

Shuttleworth, W. J.: Terrestrial Hydrometeorology, Wiley-Blackwell, West Sussex, 1 edn., doi:10.1002/9781119951933, 2012.

Stewart, J.: Modelling surface conductance of pine forest, Agricultural and Forest Meteorology, 43, 19–35, doi:10.1016/0168-1923(88)90003-2, 1988.

Sutanto, S. J., van den Hurk, B., Hoffmann, G., Wenninger, J., Dirmeyer, P. A., Seneviratne, S. I., Röckmann, T., Trenberth, K. E., and Blyth, E. M.: HESS Opinions: A perspective on different approaches to determine the contribution of transpiration to the surface moisture fluxes, Hydrology and Earth System Sciences Discussions, 11, 2583–2612, doi:10.5194/hessd-11-2583-2014, 2014.

Syed, T. H., Famiglietti, J. S., Chambers, D. P., Willis, J. K., and Hilburn, K.: Satellite-based global-ocean mass balance estimates of interannual variability and emerging trends in continental freshwater discharge., Proceedings of the National Academy of Sciences of the United States of America, 107, 17 916–21, doi:10.1073/pnas.1003292107, 2010.

Teuling, A. J., Seneviratne, S. I., Williams, C., and Troch, P. A.: Observed timescales of evapotranspiration response to soil moisture, Geophysical Research Letters, 33, L23 403, doi:10.1029/2006GL028178, 2006.

Teuling, A. J., Seneviratne, S. I., Stöckli, R., Reichstein, M., Moors, E., Ciais, P., Luyssaert, S., van den Hurk, B. J. J. M., Ammann, C., Bernhofer, C., Dellwik, E., Gianelle, D., Gielen, B., Grünwald, T., Klumpp, K., Montagnani, L., Moureaux, C., Sottocornola, M., and Wohlfahrt, G.: Contrasting response of European forest and grassland energy exchange to heatwaves, Nature Geoscience, 3, 722–727, doi:10.1038/ngeo950, 2010.

Tobón Marin, C., Bouten, W., and Sevink, J.: Gross rainfall and its partitioning into throughfall, stemflow and evaporation of intercepted water in four forest ecosystems in western Amazonia, Journal of Hydrology, 237, 40–57, doi:10.1016/S0022-1694(00)00301-2, 2000.

Tourula, T. and Heikinheimo, M.: Modelling evapotranspiration from a barley field over the growing season, Agricultural and Forest Meteorology, 91, 237–250, doi:10.1016/S0168-1923(98)00065-3, 1998.

Trenberth, K. E.: Changes in precipitation with climate change, Climate Research, 47, 123–138, doi:10.3354/cr00953, 2011.

Trenberth, K. E., Smith, L., Qian, T., Dai, A., and Fasullo, J. T.: Estimates of the Global Water Budget and Its Annual Cycle Using Observational and Model Data, Journal of Hydrometeorology, 8, 758–769, doi:10.1175/JHM600.1, 2007.

Tshimanga, R. M.: Hydrological uncertainty analysis and scenario-based streamflow modelling for the Congo River Basin, Ph.D. thesis, Rhodes University, http://eprints.ru.ac.za/2937/1/

TSHIMANGA-PhD-TR12-49.pdf, 2012.

Tuinenburg, O. A.: Atmospheric Effects of Irrigation in Monsoon Climate: The Indian Subcontinent, Ph.D. thesis, Wageningen University, 2013.

Twine, T. E., Kustas, W. P., Norman, J. M., Cook, D. R., Houser, P. R., Meyers, T. P., Prueger, J. H., Starks, P. J., and Wesley, M. L.: Correcting eddy-covariance flux underestimates over a grassland, Agricultural and Forest Meteorology, 103, 279–300, 2000.

van den Hoof, C., Vidale, P. L., Verhoef, A., and Vincke, C.: Improved evaporative flux partitioning and carbon flux in the land surface model JULES: Impact on the simulation of land surface processes in temperate Europe, Agricultural and Forest Meteorology, 181, 108–124, doi:10.1016/j.agrformet.2013.07.011, 2013.

van den Hurk, B. J. J. M.: Impact of leaf area index seasonality on the annual land surface evaporation in a global circulation model, Journal of Geophysical Research, 108, 4191, doi:10.1029/2002JD002846, 2003.

van den Hurk, B. J. J. M., Viterbo, P., Beljaars, A. C. M., and Betts, A. K.: Offline validation of the ERA40 surface scheme, Tech. rep., European Centre for Medium-Range Weather Forecasts (ECMWF), http://www.knmi.nl/publications/fulltexts/tm295.pdf, 2000.

van der Ent, R. J. and Savenije, H. H. G.: Length and time scales of atmospheric moisture recycling, Atmospheric Chemistry and Physics, 11, 1853–1863, doi:10.5194/acp-11-1853-2011, 2011.

van der Ent, R. J., Savenije, H. H. G., Schaefli, B., and Steele-Dunne, S. C.: Origin and fate of atmospheric moisture over continents, Water Resources Research, 46, 1–12, doi:10.1029/2010WR009127, 2010.

van der Ent, R. J., Wang-Erlandsson, L., Keys, P. W., and Savenije, H. H. G.: Contrasting roles of interception and transpiration in the hydrological cycle. Part II: Moisture recycling, Earth System Dynamics Discussions, p. submitted, 2014.

Vinukollu, R. K., Meynadier, R., Sheffield, J., and Wood, E. F.: Multi-model, multi-sensor estimates of global evapotranspiration: climatology, uncertainties and trends, Hydrological Processes, 25, 3993–4010, doi:10.1002/hyp.8393, 2011.

Wang, A., Zeng, X., Shen, S. S., Zeng, Q.-C., and Dickinson, R. E.: Time Scales of Land Surface Hydrology, Journal of Hydrometeorology, 7, 868–879, doi:10.1175/JHM527.1, 2006.

Wang, D., Wang, G., and Anagnostou, E. N.: Evaluation of canopy interception schemes in land surface models, Journal of Hydrology, 347, 308–318, doi:10.1016/j.jhydrol.2007.09.041, http://linkinghub.elsevier.com/retrieve/pii/S0022169407004866, 2007.

Wei, J., Dirmeyer, P. A., Wisser, D., Bosilovich, M. G., and Mocko, D. M.: Where Does the Irrigation Water Go? An Estimate of the Contribution of Irrigation to Precipitation Using MERRA, Journal of Hydrometeorology, 14, 275–289, doi:10.1175/JHM-D-12-079.1, 2013.

Wilson, K., Goldstein, A., Falge, E., Aubinet, M., Baldocchi, D., Berbigier, P., Bernhofer, C., Ceulemans, R., Dolman, H., Field, C., Grelle, A., Ibrom, A., Law, B., Kowalski, A., Meyers, T., Moncrieff, J., Monson, R., Oechel, W., Tenhunen, J., Valentini, R., and Verma, S.: Energy balance closure at FLUXNET sites, Agricultural and Forest Meteorology, 113, 223–243, doi:10.1016/S0168-1923(02)00109-0, 2002.

Xiao, J., Chen, J., Davis, K. J., and Reichstein, M.: Advances in upscaling of eddy covariance measurements of carbon and water fluxes, Journal of Geophysical Research, 117, G00J01, doi:10.1029/2011JG001889, 2012.

Zeng, X.: Global Vegetation Root Distribution for Land Modeling, Journal of Hydrometeorology, 2, 525–530, doi:10.1175/1525-7541(2001)002<0525:GVRDFL>2.0.CO;2, 2001.

Zhou, M., Ishidaira, H., Hapuarachchi, H., Magome, J., Kiem, A., and Takeuchi, K.: Estimating potential evapotranspiration using Shuttleworth–Wallace model and NOAA-AVHRR NDVI data to feed a distributed hydrological model over the Mekong River basin, Journal of Hydrology, 327, 151–173, doi:10.1016/j.jhydrol.2005.11.013, 2006.